NONLINEAR FINITE ELEMENT ANALYSIS OF MULTILAYERED BEAM-COLUMNS

by

Rajesh Chandra

B. Tech. (Hons.), Indian Institute of Technology, Kharagpur, India

A THESIS SUBMITTED IN PARTIAL FULFILLMENT OF

THE REQUIREMENTS FOR THE DEGREE OF

MASTER OF APPLIED SCIENCE

in

THE FACULTY OF GRADUATE STUDIES

CIVIL ENGINEERING

We accept this thesis as conforming

to the required standard

THE UNIVERSITY OF BRITISH COLUMBIA

October,1989

In presenting this thesis in partial fulfilment of the requirements for an advanced degree at the University of British Columbia, I agree that the Library shall make it freely available for reference and study. I further agree that permission for extensive copying of this thesis for scholarly purposes may be granted by the head of my department or by his or her representatives. It is understood that copying or publication of this thesis for financial gain shall not be allowed without my written permission.

Department of Civil Engineering
The University of British Columbia
Vancouver, B.C., CANADA V6T 1W5
October,1989

Abstract

A finite element model has been developed in this thesis for predicting strength and stiffness behavior of multilayered beam-columns. The analysis incorporates material and geometric nonlinearities in order to determine the ultimate load carrying capacity. The finite element model takes into account the continuous variability of material properties along the length of layers so that multilayered wood beam-columns can be analyzed. Transverse as well as lateral bending in combination with axial tension or compression can be considered along with different layer configurations, various support and loading conditions.

A computer program has been developed based on this formulation. Cubic beam elements have been used. Numerical integration of the virtual work equations has been carried out using Gauss quadrature. The resulting set of nonlinear equations is solved by using the Newton-Raphson scheme.

Numerical investigations have been carried out to verify the results and test the capabilities of the program.

Table of Contents

Tables

Figures

Acknowledgement

My special thanks to my supervisor Dr. Ricardo O. Foschi, for his guidance and encouragement throughout the course of my research work and in the preparation of this thesis. I would also like to thank Felix Z. Yao, Bryan Folz, James D. Dolan and all my friends of the Civil Engineering Department, UBC, for their support and valuable suggestions.

Financial support in the form of a Research Assistantship from the Natural Sciences and Engineering Research Council of Canada is gratefully acknowledged.

To

My Parents

Kamla and Akhilesh Chandra

CHAPTER 1

Introduction and Literature Review

1.1 General Remarks

The use of glued-laminated multilayered beams and beam-columns is quite common in timber buildings and could be used increasingly in larger commercial and industrial structures. Analysis and design methods for biaxial bending and axial loading are simplistic and do not represent the true behavior of the composite beam. With the advent of computers, however, it is feasible to incorporate ultimate strength analysis and design. Also, reliability methods are being used in revising the timber codes in Canada and elsewhere. The present study attempts to provide a more rigorous analysis tool for beam-columns under biaxial bending and axial loading.

It has been customary to treat a three-dimensional structure as a collection of two-dimensional, planar structures. Although this kind of idealization has resulted in satisfactory designs, it may not allow for an optimum design. The main reason for this simplification has been the complexities involved in three dimensional analysis and the difficulties involved in their hand calculations. However, with computers being widely used in structural engineering, such analyses have become easier and more accurate.

Beam-columns are often subjected to biaxial bending coupled with tension or compression. This may result from the space action of the entire framing system or by an axial load eccentrically located with respect to the principal axes of a beam-column cross section, as shown in Figs. 1.1(a) and 1.1(b). Although the two loading conditions

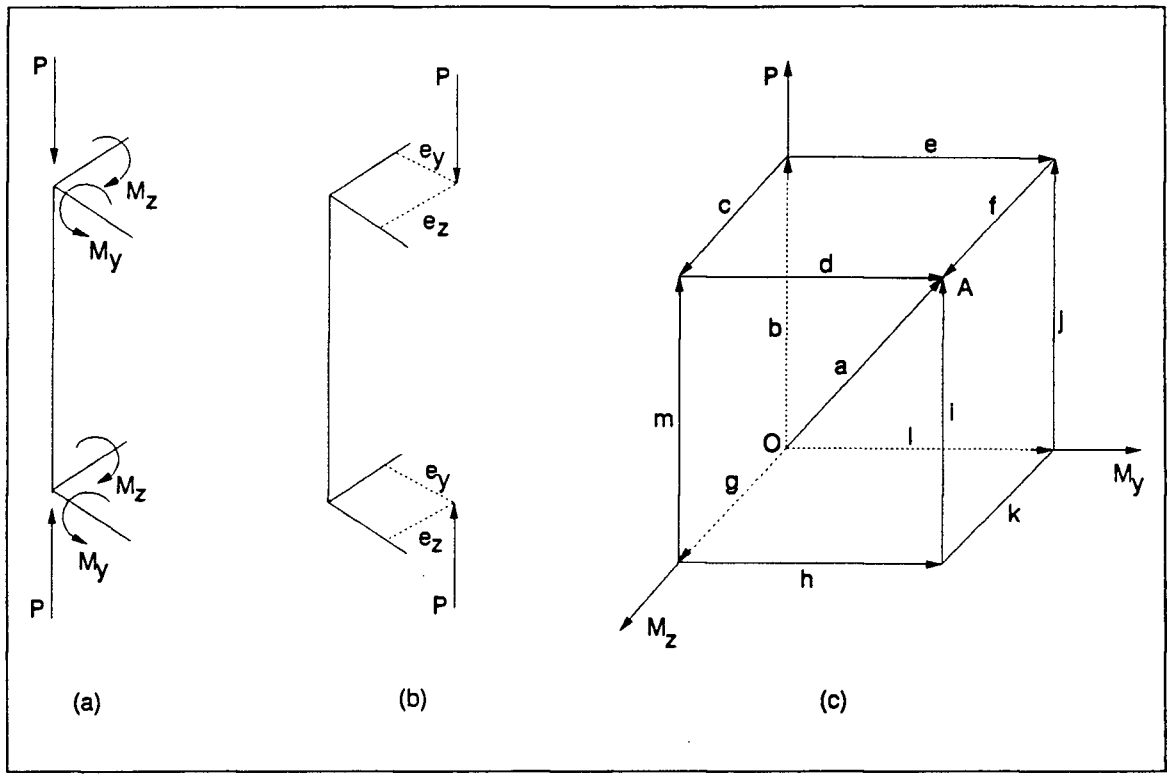

Figure 1.1: Biaxial loading on beam-column

shown above are statically equivalent and are considered identical, their nonlinear behavior may be quite different depending on the history of loading. However, in the present analysis, such differences in loading history have been ignored largely because of the unavailability of data on such stress reversals and failure modes. Recent studies by Buchanan [5] and others have tried to address this issue. In the present analysis monotonically increasing loads have been considered and load reversals have not been allowed. It is also of interest to note that the failure in the beam-column may be caused following one of the several paths shown in Fig. 1.1(c). For example the bending moment in y-direction M_y may be applied first up to a certain value following path l, then the bending moment in z-direction M_z may be applied upto a certain value following path k, and then finally the axial loading P may be increased following path i until the beam-column fails. The failure may also be caused following paths ghi, bcd or any other path as shown in Fig. 1.1(c). The two loading conditions

as shown in Figs. 1.1(a) and 1.1(b) are different and the response of the beam-column will vary depending on the load history. However, if P, M_x, M_y increase proportionally as radial loading, the two loading conditions are equivalent. In the present study, this proportional increase in loading has been used.

Wood being an organic building material, the modulus of elasticity, tensile and compressive strengths have large variability, both within and across members. This variability in material properties of wood makes an accurate design procedure difficult and the performance of such wood structures more uncertain. In recent years, this uncertainty has been addressed by using reliability based design procedures in wood structures. Timber codes are being revised to incorporate this change in design philosophy.

The present study was undertaken to develop a general analysis tool for multilayered beams and beam-columns, with a specific application to glued-laminated beam-columns. Koka [17] has developed such a model for solid wood beam-columns. However it has limitations of being a planar model, i. e. bending in only one direction, lacking the capability of torsional analysis and can only handle a solid (i. e. single layered) beam-column. The model FENMBC (Finite Element Nonlinear analysis of Multilayered Beam-Columns) developed in the present study was to overcome these limitations. It is based on a 3-dimensional analysis including axial deformation, biaxial bending and torsion for multilayered beam columns. Both geometric and material nonlinearities were incorporated in order to be able to predict ultimate load carrying capacities.

Foschi and Barrett [9] developed a model for predicting the strength and stiffness of glued-laminated beams. In this model, each lamination of thickness t is divided into cells of depth t and width W, and 6 inches ($152mm$) in length. Each cell is randomly assigned a density and a knot diameter from knot frequency data for the specific lamination in consideration. A modulus of elasticity (MOE) and a tensile

strength value is assigned to each cell. The model uses a linear finite element method to obtain stresses in each cell, considering each one a five noded plate element. The model uses weakest link failure criterion to calculate the strength of the beam.

The Foschi/Barrett model formed the basis for the development of the Karlsruhe model [7]. This finite element model takes into account the material nonlinearity of wood in compression, by using a linear elasto-plastic stress-strain relationship. It then considers the successive failure of cells in the tension zone.

For the past few years research work has also been done in the area of simulation of material properties of lumber, particularly within board variations in modulus of elasticity and strength. (Bender et al. [3], Foschi [10], Taylor and Bender [28] and Colling [7]). The simulation of material properties of built-up beam-columns is not the objective of the present study. The analysis assumes that these material properties of all laminations are given, or can be simulated along their length.

The stress-strain relationship used herein are discussed in detail in Section 2.3 in Chapter 2, however, a brief survey of axial tension strength of timber has been presented here. It was not until the mid-seventies that the axial tensile strength of timber was given much attention. This was due to the lack of suitable connection details which prevented very high stresses from being developed in tension members. With the availability of more effective connections, there was a renewed interest in tensile strength of timber. The phenomenon of size effect was observed by Kunesh and Johnson [18] (1974). They tested commercial sizes of clear Douglas-fir and Hem-fir and noticed a significant decrease in tensile strength with increasing cross-sectional dimensions.

Norris [23] (1955), Dawe [8] (1964), Nemeth [22] (1965) and others have contributed to the development of appropriate theory dealing with defects in timber. The effect of defects in timber was also ignored in the belief that modulus of rupture was a conservative estimate of tension strength. There was a renewed interest in

this area after in-grade testing showed failures occuring at stresses much lower than the modulus of rupture. Since then there has been considerable research work done in this area. A general finding from these studies was that the large knots reduced the strength more than smaller knots, and edge knots more than center knots, a result confirmed by Kunesh and Johnson [19] (1972) and Johnson and Kunesh [16] (1975). Attempts have been made to combine various characteristics such as knot size, flexural stiffness and slope of grain to predict tensile strength.

1.2 Objectives

This study aimed at the following objectives:

1. Development of a finite element analysis model for predicting strength and stiffness behavior of multilayered beam-columns. This analysis would include nonlinear material and geometric behavior of the beam-column so that the ultimate load carrying capacity can be determined. The finite element model would take into account the continuous variability of material properties along the length. The loading would be axial, transverse and lateral as in a three dimensional beam-column.

2. Implementation of this analysis into a computer program which would allow flexibility in placing the layers in different configurations, various support conditions and loadings. It would also be user friendly and would require a minimum of data input.

3. Validation of this computer program by comparing its predictions with available analytical or experimental results.

1.3 Thesis Organisation

Chapter 2 describes the formulation of the theory used in the development of the multilayered beam-column model. The general assumptions, kinematic and constitutive relationships are given in detail.

Chapter 3 provides the outline and detail of the finite element formulation of the problem and the computer implementation. The virtual work equations have been set up and the Newton-Raphson iteration technique has been employed to solve the nonlinear equations. Gauss quadrature scheme has been employed for the numerical integration. The details of convergence criterion have been outlined.

Chapter 4 compares the predictions of this program with available results wherever possible and presents cases including stability and strength analysis.

Chapter 5 includes conclusion of the present study and recommendations for further research work in this area.

CHAPTER 2

Formulation of Theory

2.1 General Assumptions

The assumptions made in the analysis of multilayered beam-columns are as follows:

1. Plane section remains plane (with certain qualifications as discussed later in section 2.2).

2. Solid rectangular sections are assumed for each layer and thus for the entire cross-section.

3. All layers in the beam are in constant contact with each other, thus no discontinuity exists between layers.

4. Material properties may have continuous variation along the span of a layer, however, material properties are assumed to be constant within a small division of an element (called a window as explained later in Section 3.1).

5. The stress-strain relationship has been assumed to be linear elastic with brittle failure in tension, and nonlinear having a falling branch with plastic failure in compression as shown in Fig. 2.7.

2.2 Kinematic Relationships

The orientation of the beam-column with respect to a Cartesian coordinate system is shown in Fig. 2.1. The x-axis coincides with the longitudinal axis of the beam, the

y-axis is along the lateral direction of the beam and the z-axis is along transverse direction to the beam. Let u, v and w be the displacements of the geometric center O along the x, y and z axes respectively. Let θ be the rotation of the cross-section about x-axis. Using the right-hand rule, the rotation θ is positive as shown in the Fig. 2.1.

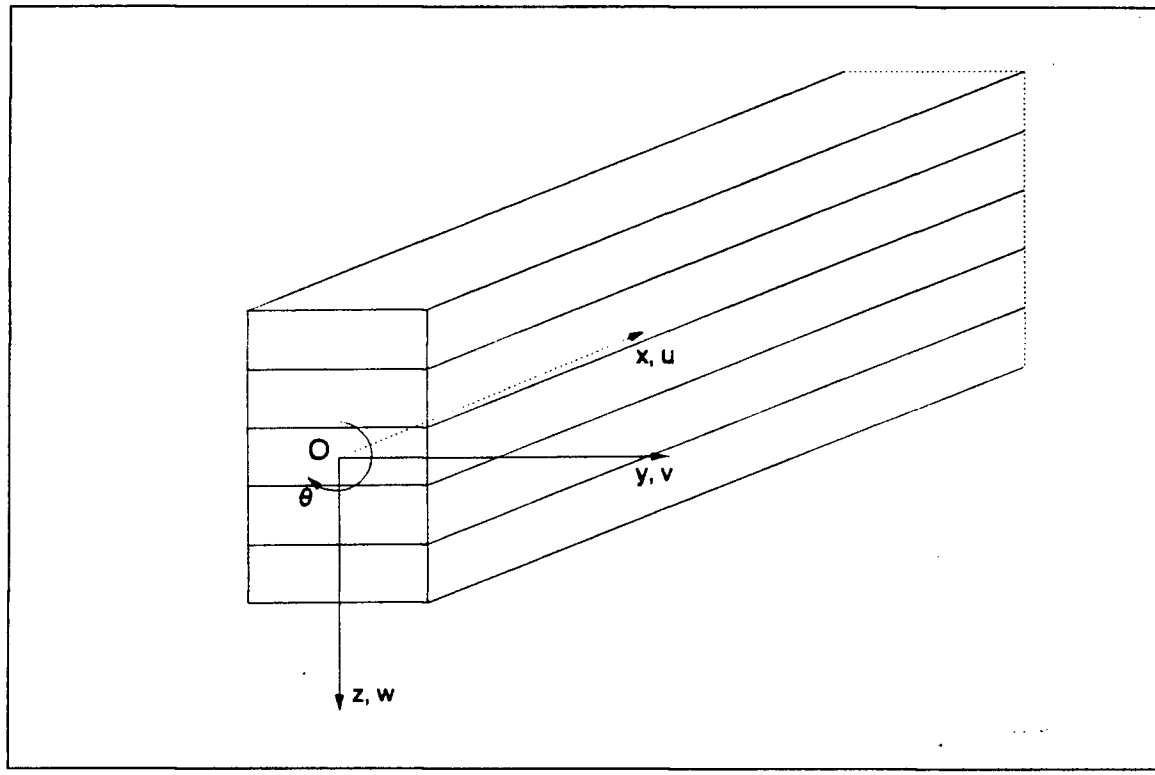

Figure 2.1: Coordinate system for the beam-column

The displacements of a generic point A on the cross-section, located at (x, y, z) are related to those of O and approximated as follows:

$$u_A = u - y\frac{dv}{dx} - z\frac{dw}{dx} + yz\frac{d\theta}{dx} \tag{2.1}$$

$$v_A = v - z\theta \tag{2.2}$$

$$w_A = w + y\theta \tag{2.3}$$

In Fig. 2.2, only the transverse deformation has been shown. It can be readily deduced from this figure that the axial deformation of point A will be reduced by

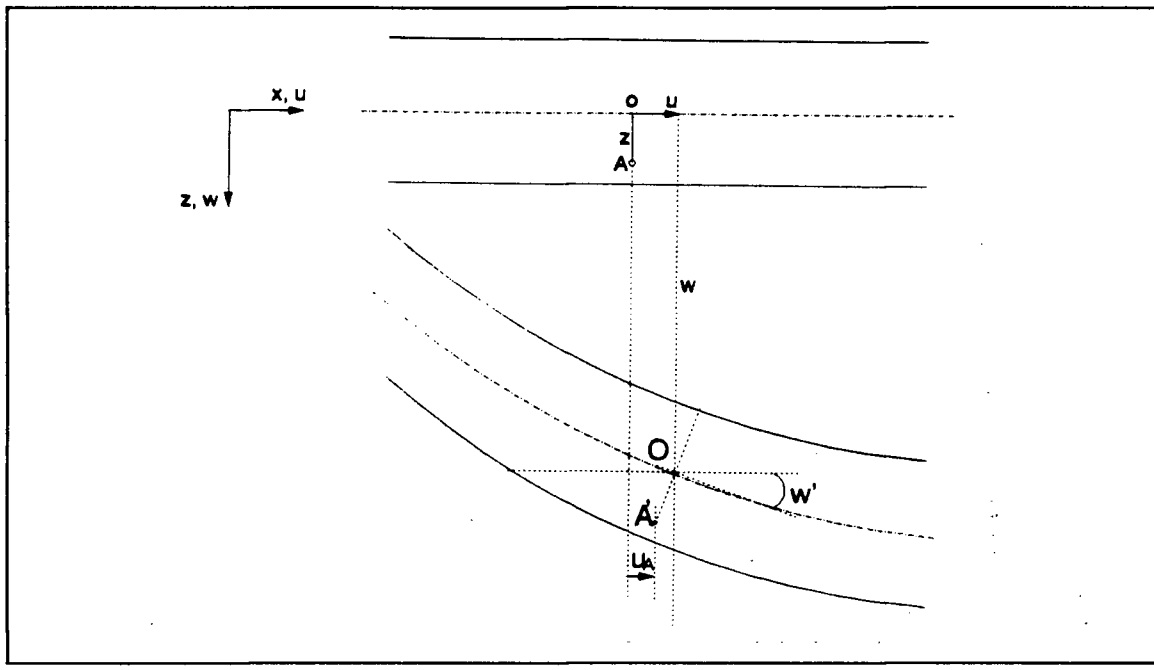

Figure 2.2: Axial and lateral displacement relationship

an amount $z\frac{dw}{dx}$ if the cross-section rotation is assumed to be the slope $\frac{dw}{dx}$ (shear deformation neglected). A similar argument can be employed for the second term in Eq.(2.1) by replacing w and z with v and y respectively. The last term in Eq.(2.1) has been included to account for warping of the cross-section due to the rotation θ.

The nonlinear strain-displacement relationship used in the present study is now presented. From the geometry of the Fig. 2.3, after deformation, the change in contour length ds can be expressed as

$$ds^2 \approx dx^2[(1 + \frac{\partial u_A}{\partial x})^2 + (\frac{\partial v_A}{\partial x})^2 + (\frac{\partial w_A}{\partial x})^2] \tag{2.4}$$

Expanding it binomially and neglecting the higher order terms, ds can be written as

$$ds = dx[1 + \frac{\partial u_A}{\partial x} + \frac{1}{2}(\frac{\partial v_A}{\partial x})^2 + \frac{1}{2}(\frac{\partial w_A}{\partial x})^2] \tag{2.5}$$

Thus the axial strain ε can be expressed as

$$\varepsilon = \frac{ds - dx}{dx} = \frac{\partial u_A}{\partial x} + \frac{1}{2}(\frac{\partial v_A}{\partial x})^2 + \frac{1}{2}(\frac{\partial w_A}{\partial x})^2 \tag{2.6}$$

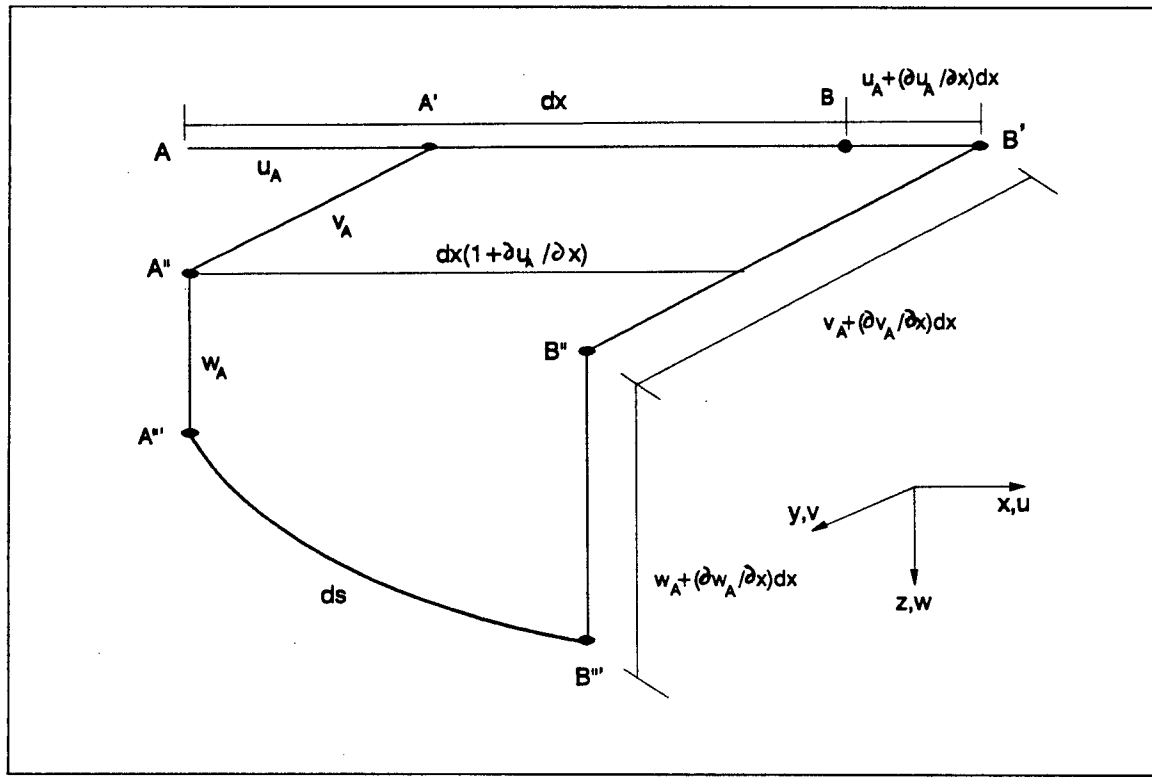

Figure 2.3: Large deformation relationships

Substituting u_A, v_A and w_A from Eqs.(2.1), (2.2) and (2.3), the strain displacement for a general point in the beam-column is given by

$$\begin{aligned}\varepsilon &= \frac{du}{dx} - y(\frac{d^2v}{dx^2} - z\frac{d^2\theta}{dx^2}) - z\frac{d^2w}{dx^2} \\ &\quad +\frac{1}{2}(\frac{dv}{dx} - z\frac{d\theta}{dx})^2 + \frac{1}{2}(\frac{dw}{dx} + y\frac{d\theta}{dx})^2 \end{aligned} \tag{2.7}$$

2.3 Stress-Strain Relationships

While wood is assumed to behave elastically in tension as discussed earlier in Section 1.1, many uniaxial stress-strain relationships have been proposed by various researchers to model the nonlinear behaviour of wood in compression. These are mostly empirical in nature, attempting to theoretically represent the stress-strain relationships obtained from laboratory testing of different types of wood. In this section, the important stress-strain relationships in compression applicable to wood structures are

reviewed first and then the one used in the present analysis is discussed.

A simple elastic-perfectly plastic bilinear approximation as shown in Fig. 2.4 has been used quite often to calculate the ultimate load carrying capacity of wood members.

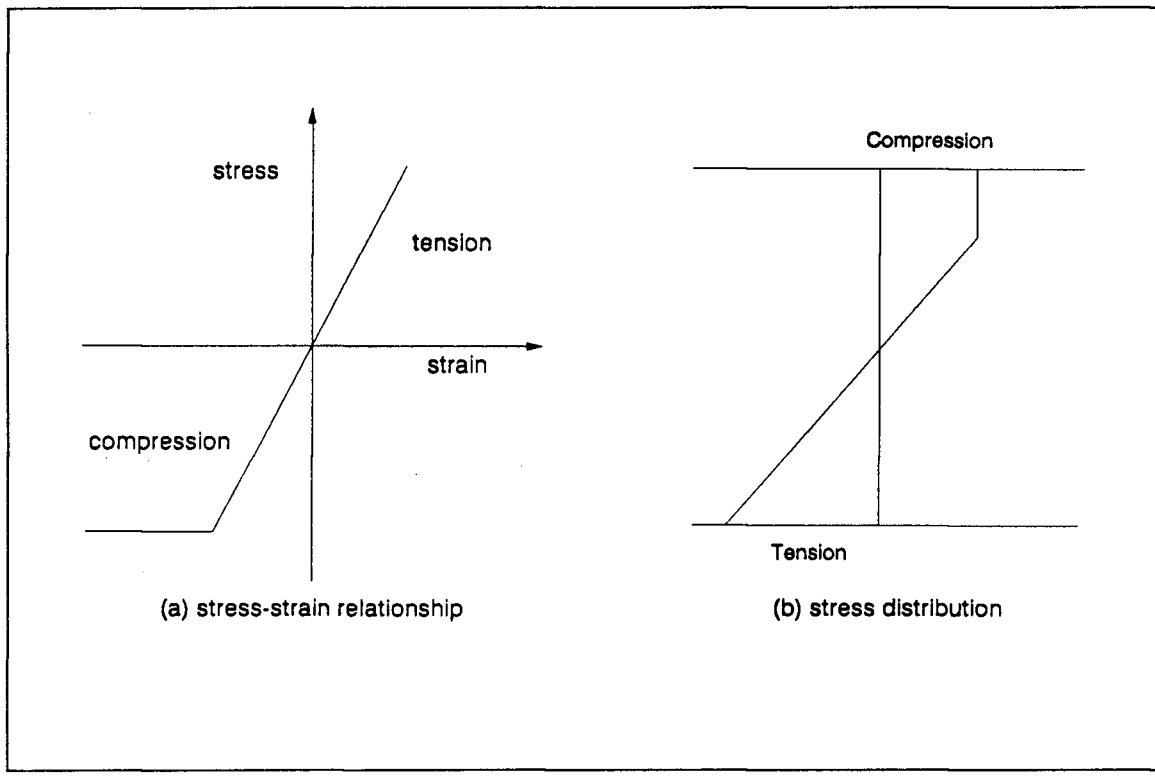

Figure 2.4: Bilinear elasto-plastic stress-strain relationship

Ylinen [29] (1956) proposed a simple bilinear relationship, which was used by Malhotra and Mazur [20] (1971) in their research work. This relationship can be given as

$$\varepsilon = \frac{1}{E}[c\sigma - (1-c)f_c ln(1 - \frac{\sigma}{f_c})] \tag{2.8}$$

where ε is the normal strain, σ is the normal stress, f_c is maximum compressive stress, E is the initial modulus of elasticity and c is a parameter depending on the shape of the curve. As can be readily found out, the curve described by Eq.(2.8) and shown in Fig. 2.5a is tangent to the elastic modulus at the origin and tangent to the ultimate compressive stress for large strain.

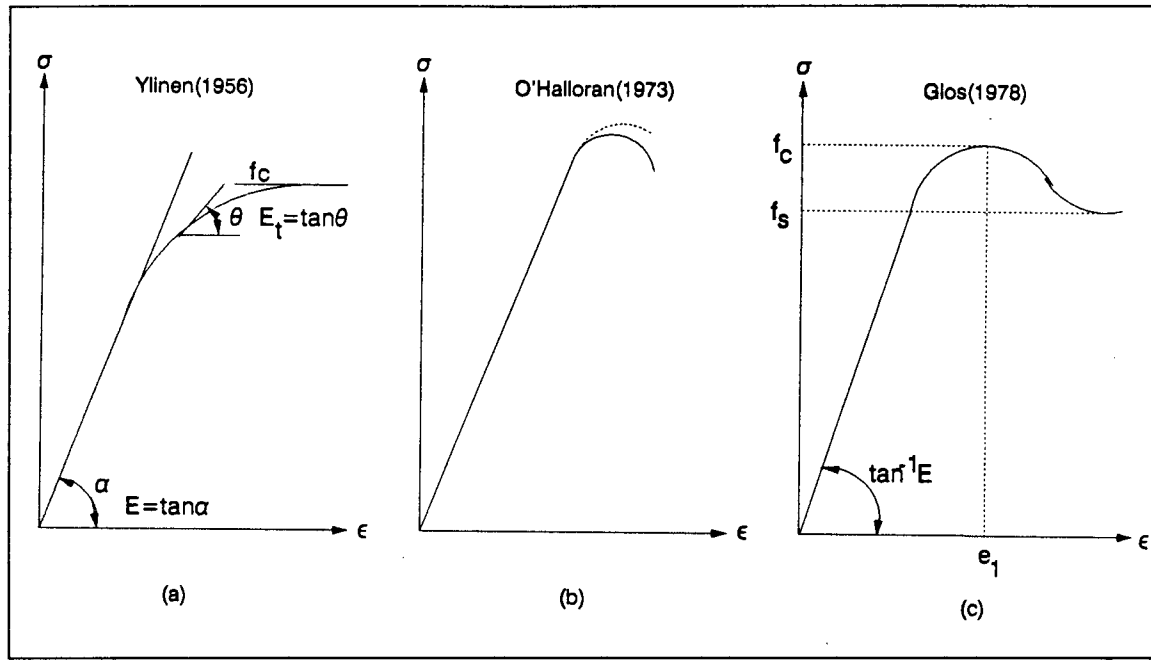

Figure 2.5: Various stress-strain relationships

Malhotra and Mazur [20] have used this relationship extensively to predict the buckling strength of solid timber columns and described the curve as a good approximation to the results of laboratory testing of 144 clear eastern spruce wood having different moisture contents. However they have not considered the shape of the curve beyond the ultimate load.

Goodman and Bodig [15] (1971) carried out extensive tests on clear dry wood in compression parallel to the grain and reported the test results. O'Halloran [24] (1973) has used these data to propose a mathematical equation for the stress-strain curve at various grain angles and grain orientations. This equation has been given in the form

$$\sigma = E\varepsilon - A\varepsilon^n \tag{2.9}$$

where σ is stress, ε is strain, E modulus of elasticity, A and n are equation constants determined by fitting the equation to a given set of experimental data. If the strain at peak stress is found to a certain ratio, r, of equivalent strain under elastic conditions,

the parameter A and n can be found from

$$n = \frac{r}{r-1} \tag{2.10}$$

$$A = \frac{E}{n(\frac{rf_c}{E})^{n-1}} \tag{2.11}$$

where f_c is the maximum stress.

A typical plot of the fitted curve is shown in Fig. 2.5(b). The equation cannot be used beyond the maximum compressive stress f_c, because it drops rapidly to negative stress values. O'Halloran claims that this is not a serious problem failing to recognize that the shape of the falling branch of the curve is needed to predict the ultimate bending strength. It is true that the stress-strain relationship beyond maximum load cannot be qualified easily in an axial compression test, because it is largely a function of the test machine characteristics and the rate of loading, but a description of stress-strain behaviour beyond ultimate load is essential to the development of an ultimate bending strength theory.

A simple bilinear proposal by Bazan [2] (1980) has been illustrated in Fig. 2.6. Bazan assumed without any supporting argument that the slope of the falling branch is a variable which can be arbitrarily taken as that value which produces maximum bending moment for any neutral axis depth. A different assumption used by Buchanan [5] (1984) is that the slope of the falling branch is a material property which can be estimated as part of the calibration of the computer model to test results.

A comprehensive study of the stress-strain relationship of timber with defects, in compression parallel to the grain, has been made by Glos [14] (1978). On the basis of extensive experimental testing, Glos proposed a curve of the shape shown in Fig. 2.5 which is similar to that reported for clear wood by Bechtel and Norris [4] (1952), Moe [21] (1961) and others. The curve is characterized by four parameters as shown in Fig. 2.7. The equation of the curve is given by

$$f = \frac{\frac{\epsilon}{\epsilon_1} + G_1(\frac{\epsilon}{\epsilon_1})^7}{G_2 + G_3(\frac{\epsilon}{\epsilon_1}) + G_4(\frac{\epsilon}{\epsilon_1})^7} \tag{2.12}$$

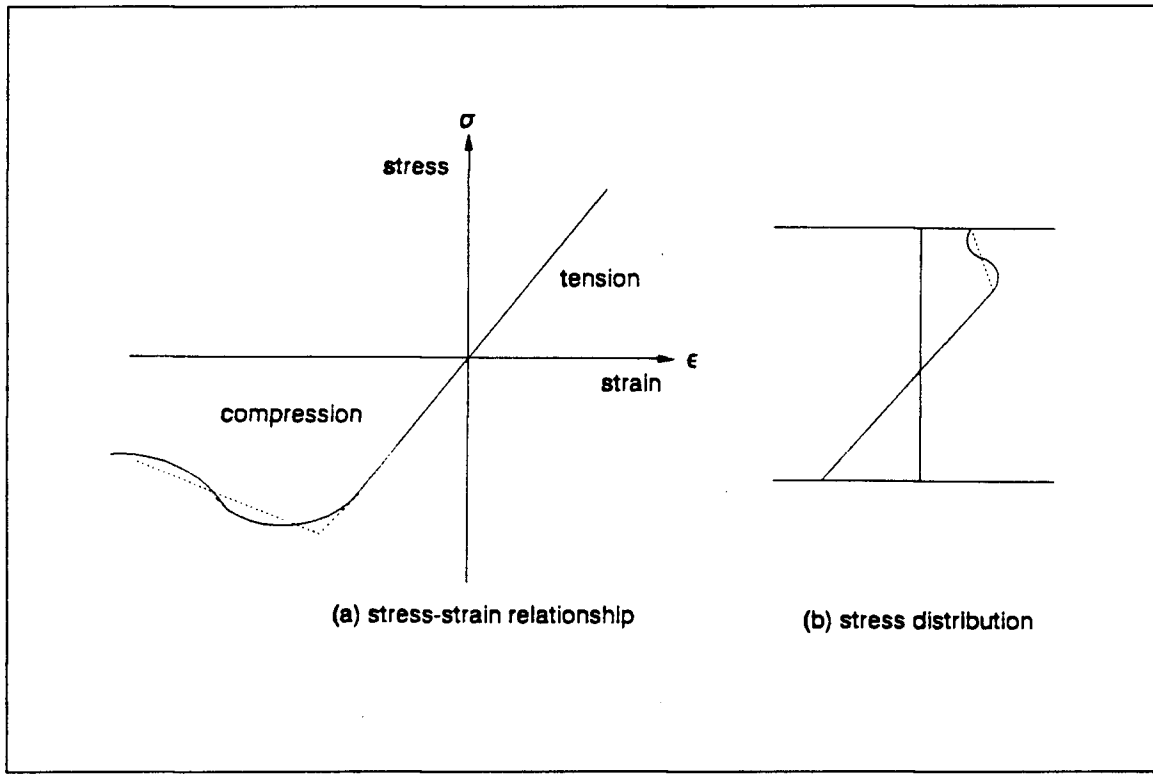

Figure 2.6: Bilinear stress-strain relationship proposed by Bazan (1980)

where

$$
\begin{aligned}
G_1 &= \frac{f_s}{6E(1-\frac{f_s}{f_c})} \\
G_2 &= \frac{1}{E} \\
G_3 &= \frac{1}{f_c} - \frac{7}{6E} \\
G_4 &= \frac{G_1}{f_s}
\end{aligned}
$$

where f is the stress, e is strain, E is modulus of elasticity, f_c is maximum compressive stress, f_s is the asymptotic compression stress for large strain and e_1 is the strain at maximum stress.

Glos has estimated the four parameters to define the shape of the curve from four measurable wood properties: density, moisture content, knot ratio and percentage

compression wood. Multiple curvilinear regression techniques have been used to express expected values of each parameter in terms of the four properties, using length regression equations.

Koka [17] (1987) has used the bilinear stress-strain relationship as proposed by Bazan [2] and later modified by Buchanan [5] (1984), who pointed out that the slope of the falling branch of the stress-strain relationship is considered to be a material property. Koka has used the following relationship

$$\sigma = E_0\varepsilon - [E_0\varepsilon + |f_c|(1+m) + mE_0\varepsilon](1 - \Delta(\varepsilon + |\varepsilon_c|)) \tag{2.13}$$

where σ is stress, E_0 is elasticity modulus, ε is strain, f_c is maximum compressive stress, m is the slope of the falling branch on compression side, ε_c is the maximum strain corresponding to the maximum compressive stress f_c and $\Delta(\varepsilon + |\varepsilon_c|)$ is the step function defined as follows

$$\varepsilon \geq -|\varepsilon_c| \Rightarrow \Delta(\varepsilon + |\varepsilon_c|) = 1 \tag{2.14}$$

$$\varepsilon \leq -|\varepsilon_c| \Rightarrow \Delta(\varepsilon + |\varepsilon_c|) = 0 \tag{2.15}$$

The bilinear relationship for different values of m has been shown in Fig. 2.8.

A further extension of this relationship was made to obtain a more realistic approximation of the stress-strain behaviour of wood in compression parallel to the grain by employing an exponential variation on the compression side. On the tension side, the stress-strain varies linearly and elastically up to a maximum tensile stress F_t, upon which a brittle failure occurs.

$$\sigma = E\varepsilon - [E\varepsilon - F(\varepsilon)](1 - \Delta(\varepsilon)) \tag{2.16}$$

The function $F(\varepsilon)$ for $\varepsilon < 0$ has the form

$$F(\varepsilon) = [-|p_0| - m_1 E\varepsilon](1 - e^{\frac{E\varepsilon}{|p_0|}}) \tag{2.17}$$

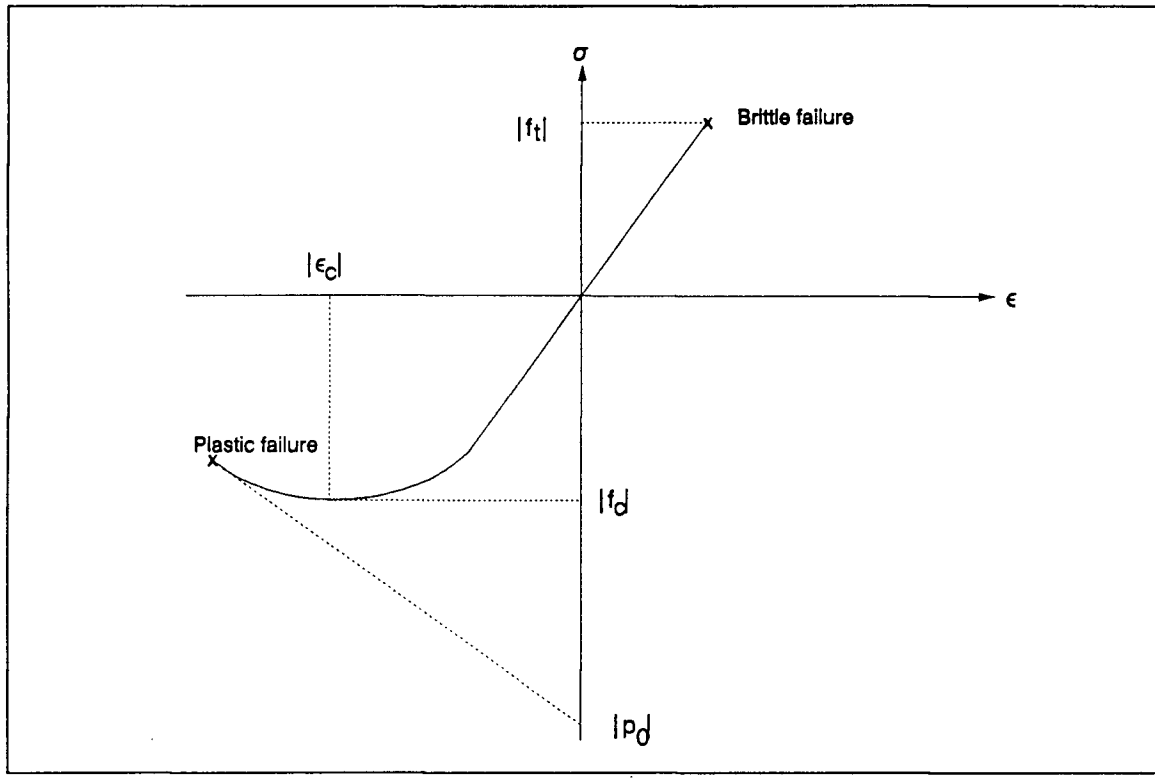

Figure 2.7: Stress-strain relationship used in the present study

In Eqs.(2.16) and (2.17) above, σ is the stress, E is the modulus of elasticity, ε is the strain, $|p_0|$ is the intercept on the stress axis resulting from the extrapolation of the tangent to the falling branch of the stress-strain relationship as shown in Fig. 2.7 and m_1 is the slope of the falling branch. In Eq.(2.16), $\Delta(\varepsilon)$ is a step function which can be defined as follows

$$\Delta(\varepsilon) = \begin{cases} 1, & \text{if } \varepsilon > 0 \\ 0, & \text{if } \varepsilon < 0 \end{cases} \tag{2.18}$$

In Eq.(2.16) only the three parameters E, f_c and m_1 need be specified. The remaining parameters of the equation can be calculated in the following manner. From Eq.(2.16), for $\varepsilon = \varepsilon_c$ the following expression can be readily obtained

$$[-|p_0| - m_1 E\varepsilon_c](1 - e^{\frac{E\varepsilon_c}{|p_0|}}) = -|F_c| \tag{2.19}$$

Differentiating Eq.(2.16) with respect to ε and substituting $\varepsilon = \varepsilon_c$, the following

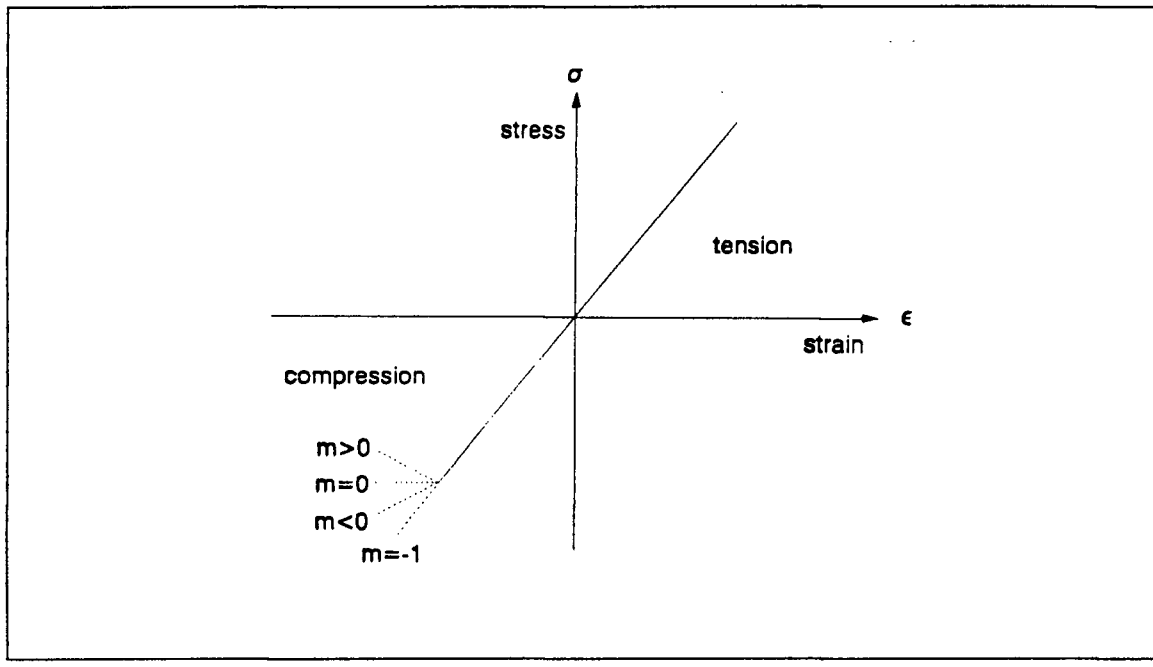

Figure 2.8: Bilinear stress-strain relationships for various m as used by Koka

equation can be obtained

$$-m_1E(1-e^{-\frac{E}{|p_0|}|\varepsilon_c|})+(|p_0|-m_1E|\varepsilon_c|)\frac{E}{|p_0|}e^{-\frac{E}{|p_0|}|\varepsilon_c|}=0 \tag{2.20}$$

From Eq.(2.19),

$$|p_0|-m_1E|\varepsilon_c|=\frac{F_c}{1-e^{-\frac{E}{|p_0|}|\varepsilon_c|}} \tag{2.21}$$

Defininig

$$x=e^{-\frac{E}{|p_0|}|\varepsilon_c|} \tag{2.22}$$

and taking the logarithm of both sides,

$$lnx=-\frac{E}{|p_0|}|\varepsilon_c| \tag{2.23}$$

Substituting x into Eqs.(2.20) and (2.21), and rearranging terms,

$$-m_1E(1-x)+\frac{F_c}{1-x}\frac{E}{|p_0|}x=0 \tag{2.24}$$

Since from Eq.(2.24), $|p_0|$ can be written as

$$|p_0|=|F_c|\frac{x}{m_1(1-x)^2} \tag{2.25}$$

finally, from Eqs.(2.20) and (2.25),

$$x(1 + m_1) + m_1 x ln x = m_1 \tag{2.26}$$

For a given m_1, x can be computed and from Eq.(2.23) the maximum strain $|\varepsilon_c|$ corresponding to the maximum stress F_c can be written as

$$|\varepsilon_c| = -\frac{|p_0|}{E} ln x \tag{2.27}$$

A simple iterative scheme employing Newton's method can be used to determine the unknown from Eq.(2.26). Defining the function ψ as

$$\psi = x(1 + m_1) + m_1 x ln x - m_1 \tag{2.28}$$

following the usual procedure in Newton's method, the following iterative equation can be obtained

$$x_{i+1} = x_i - \frac{x_i(1 + m_1) + m_1 x_i ln x_i - m_1}{1 + 2m_1 + m_1 ln x_i} \tag{2.29}$$

A typical stress-strain plot used in FENMBC has been shown in Fig. 2.9, corresponding to $E = 14,000 MPa, m_1 = 0.25, F_c = 140 MPa$.

The stress-strain relationship used in this study is a better representation of experimental results, as it can have a continuous curvilinear and smooth peak as opposed to the abrupt change of curvature in the simple bilinear stress-strain relationship.The falling branch can have different slopes and the failure in compression can be easily programmed. Also, the drawback of falling rapidly to negative values of the exponential stress-strain relation, as given by O'Halloran [24], has been taken care of by the variable slope m_1.

2.4 Virtual Work Equation

The Principle of Virtual Work has been used to determine the governing equilibrium equations of the beam-column. If we apply a virtual displacement $\delta \mathbf{a}$ to the system,

compatible with boundary conditions, the resulting internal work (δU) and external work (δW) done by the stresses and the external forces respectively are given as

$$\delta U = \int_V \delta\varepsilon^T \sigma dV \tag{2.30}$$

$$\delta W = \int_S \delta \mathbf{a}^T \mathbf{F} dS \tag{2.31}$$

where the internal work is integrated over the entire volume V and the external work is integrated over the surface area S. $\mathbf{F}$ is the external force acting per unit surface area. The principle of virtual work states that internal and external work must be equal:

$$\int_V \delta\varepsilon^T \sigma dV = \int_V \delta \mathbf{a}^T \mathbf{F} dV \tag{2.32}$$

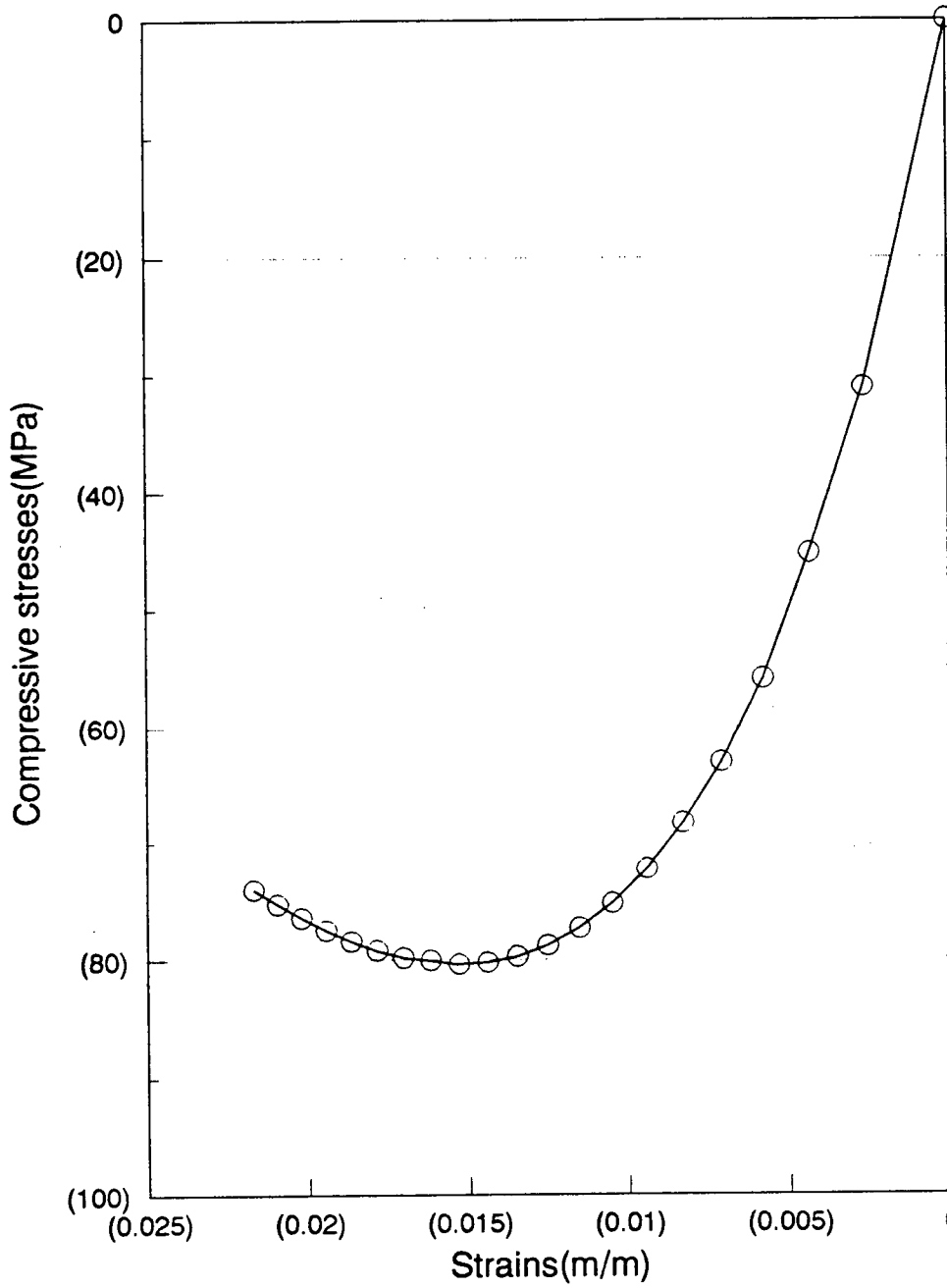

Figure 2.9: Exponential compressive stress-strain relationship used for FENMBC

CHAPTER 3

Finite Element Formulation

The basic concept underlying the finite element method is that a structure can be modelled analytically by subdividing it into a finite number of elements. Within each finite element, a set of functions are assumed to approximate the stresses or displacements in that region. The set of approximating functions contain unknown parameters and are chosen to ensure continuity throughout the system. Application of the principle of virtual work results in a system of algebraic equations for the parameters in the approximating functions.

Although finite element formulation can be based either on stress fields or displacement fields, most often a displacement based finite element formulation is applied. Such an approach is followed here. Correspondingly, the treatment for the complete structure is then accomplished by studying the stiffness matrices for the elements. The steps involved in a linear finite element analysis are

1. Discretization of the body into finite elements.

2. Evaluation of element stiffness matrices by deriving nodal force-displacement relationship.

3. Assemblage of the stiffness and force matrices for the system of elements and nodes.

4. Introduction of boundary conditions.

5. Solution of resulting equations for nodal displacements.

6. Calculation of strains and stresses based on nodal displacements.

In case of nonlinear finite element analysis, an incremental/iterative technique is required. The stiffness matrix calculated above is either updated for each load increment or the same stiffness matrix is used until the solution displacement vector converges. These procedures will be discussed in detail later in this chapter.

3.1 Finite Element Discretization

The beam-column arrangement and the finite element discretization is shown in Fig. 3.1. The span is subdivided into elements of length Δ. The layers for each element are further subdivided into windows of length Δw.The numbering of layers has been done from top to bottom. The elements are numbered from left to right and so are the windows inside every element. The nodes are also numbered from left to right. The material properties within each window are assumed to be constant and thus, a finer division would allow closer representation of a continuous variation of material properties along the span. The same could be achieved by employing a larger number of elements without windows, but then a larger stiffness matrix would be obtained. Thus while keeping the size of the stiffness matrix within reasonable limits, the concept of windows permits consideration of the continuous variation of the material properties along the span. This results in increased efficiency of the program while solving for the displacements and stresses. Also, as this program is to be used for the ultimate load analysis involving material and geometry nonlinearities, the smaller the stiffness matrix, the greater the savings of computer time in the overall solution.

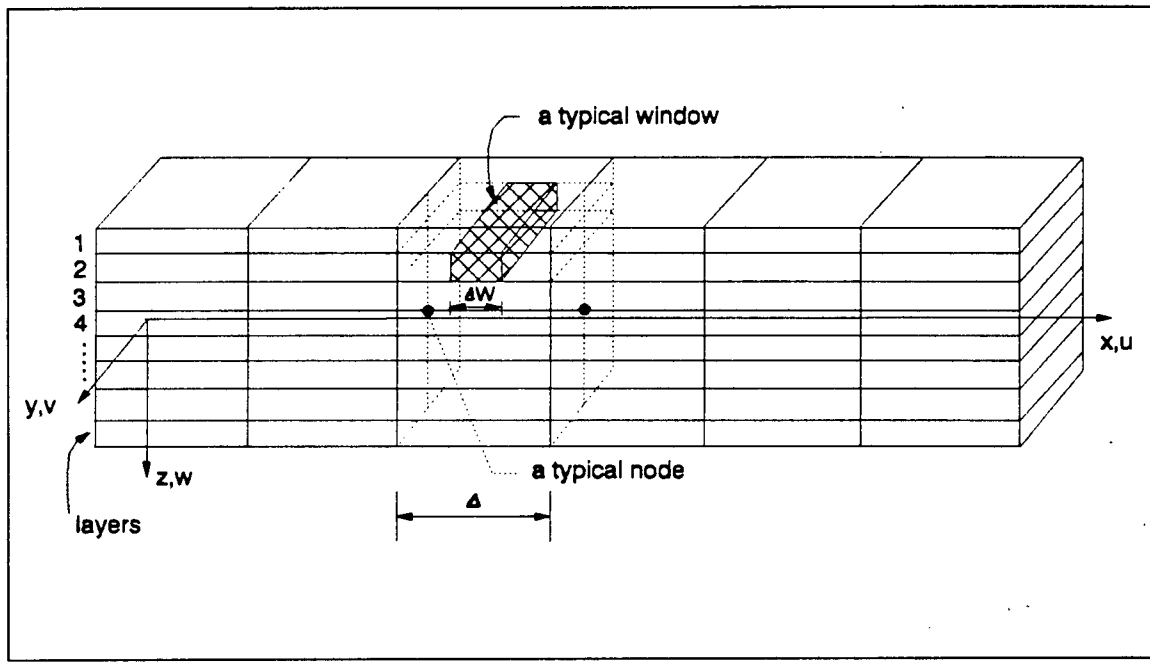

Figure 3.1: Finite element discretization of the beam-column

3.2 Problem Formulation

A beam element of length Δ with two end nodes, as shown in Fig. 3.2, is used in this formulation. A local coordinate ξ $(-1 \leq \xi \leq 1)$ is used for each element along the x-axis. The x-coordinate of any point inside the element can be expressed as

$$x = x_c + \frac{\Delta}{2}\xi \tag{3.1}$$

where x_c is the x-coordinate of the center of the element length. The element has been divided into a number of windows (NW) of equal length, hence

$$\Delta w = \frac{\Delta}{NW} \tag{3.2}$$

A second local coordinate $\eta(-1 \leq \eta \leq 1)$ is used within a window. A transformation function relating η inside the window and ξ is required (refer to Fig. 3.2), since numerical integration has to be performed inside every window and summed over the number of windows and the number of layers to obtain the element stiffness matrix.

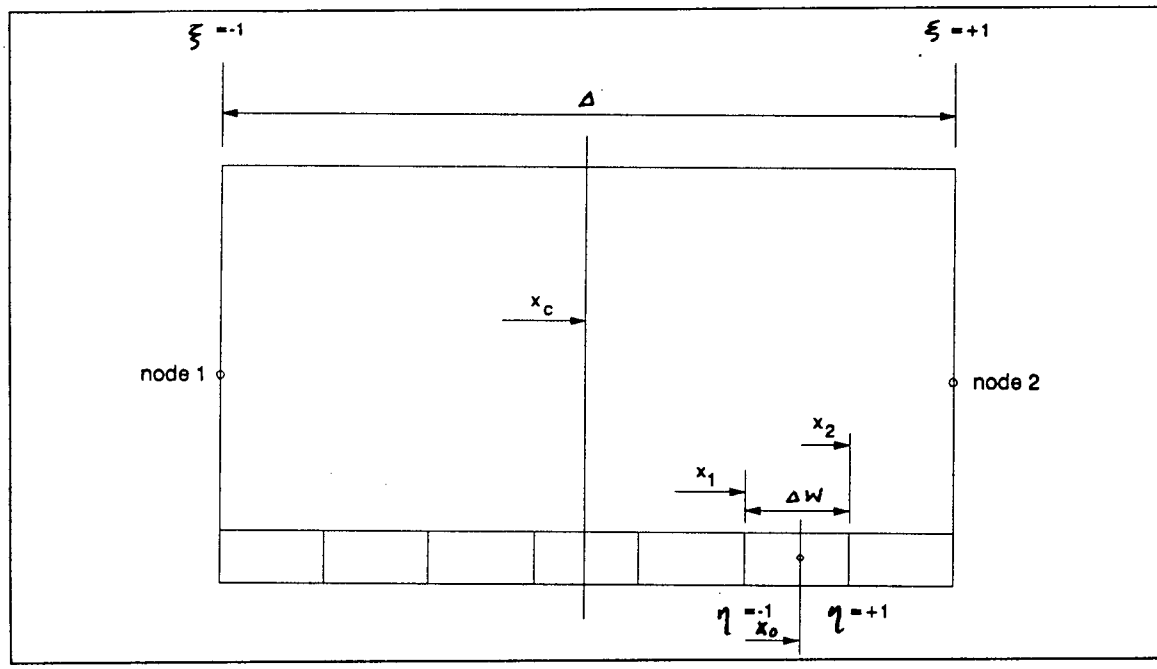

Figure 3.2: Local coordinate system for the element and the window

Thus, for the i^{th} window, Fig. 3.2,

$$x_1 = x_c - \frac{\Delta}{2} + (i-1)\Delta w = x_c + \frac{\Delta}{2}\xi_1 \tag{3.3}$$

$$x_2 = x_c - \frac{\Delta}{2} + i\Delta w = x_c + \frac{\Delta}{2}\xi_2 \tag{3.4}$$

$$x_0 = x_c - \frac{\Delta}{2} + i\Delta w - \frac{\Delta w}{2} = x_c + \frac{\Delta}{2}\xi_0 \tag{3.5}$$

From the above we can calculate ξ_1, ξ_2 and ξ_0 as

$$\xi_1 = \frac{2}{\Delta}(i-1)\Delta w - 1$$

$$\xi_2 = \frac{2}{\Delta} i\Delta w - 1$$

$$\xi_0 = \frac{2}{\Delta} i\Delta w - \frac{\Delta w}{\Delta} - 1$$

Also

$$\frac{\xi_2 - \xi_1}{2} = \frac{\Delta w}{\Delta}$$

Hence we can write ξ in terms of η as

$$\xi = (i\frac{2\Delta w}{\Delta} - \frac{\Delta w}{\Delta} - 1) + \frac{\Delta w}{\Delta}\eta \tag{3.6}$$

The displacement vector consists of nodal degrees of freedom u, v, w, θ and their first derivatives u', v', w' and θ' respectively. Thus there are eight degrees of freedom (dof) per node giving a displacement vector of sixteen dof for a beam element. The displacement vector is arranged according to the following form:

$$\mathbf{a}^T = \{u_1, u_1', v_1, v_1', w_1, w_1', \theta_1, \theta_1', u_2, u_2', v_2, v_2', w_2, w_2', \theta_2, \theta_2'\} \tag{3.7}$$

where the subscripts 1 and 2 refer to node 1 and node 2 respectively.

3.3 Interpolation Functions

To satisfy the completeness criterion, the assumed displacement field must be at least a complete polynomial of order equal to the highest derivative occurring in the strain-displacement relationship. Also the displacement function must be continuous within the element and the displacement must be compatible between adjacent elements. The compatibility condition is ensured if the displacement field is continuous on the inter-element boundary upto the derivative of one order less than the highest derivative appearing in the strain-displacement relation.

For the beam-column element the strain-displacement relationship contains second derivative in lateral displacements and twist and the first derivative in axial displacement. Hence it is necessary to choose the displacement function such that $u, u', v, v', w, w', \theta$ and θ' are continuous at nodes. This can be achieved by adopting linear displacement field for u and cubic displacements for other degrees of freedom.

However, complete cubic interpolations are used to approximate u, v, w and θ within each element. In an earlier work by Koka [17], which employed this element, it was found that a cubic interpolation function for u gives a much improved approximation of the axial stresses. A complete cubic polynomial requires 4 parameters to define the function.The displacements and their first derivatives at the two nodes provide sufficient parameters to fully describe a cubic polynomial function. Thus we

can write u, v, w and θ as

$$u = N_1 u_i + N_2(\frac{du}{dx})_i + N_3 u_j + N_4(\frac{du}{dx})_j \tag{3.8}$$

$$v = N_1 v_i + N_2(\frac{dv}{dx})_i + N_3 v_j + N_4(\frac{dv}{dx})_j \tag{3.9}$$

$$w = N_1 w_i + N_2(\frac{dw}{dx})_i + N_3 w_j + N_4(\frac{dw}{dx})_j \tag{3.10}$$

$$\theta = N_1 \theta_i + N_2(\frac{d\theta}{dx})_i + N_3 \theta_j + N_4(\frac{d\theta}{dx})_j \tag{3.11}$$

where subscripts i and j refer to the first and second nodes respectively of each element. Also

$$N_1 = (\frac{1}{2} - \frac{3}{4}\xi + \frac{1}{4}\xi^3) \tag{3.12}$$

$$N_2 = \frac{\Delta}{4}(1 - \xi - \xi^2 + \xi^3) \tag{3.13}$$

$$N_3 = (\frac{1}{2} + \frac{3}{4}\xi - \frac{1}{4}\xi^3) \tag{3.14}$$

$$N_4 = \frac{\Delta}{4}(-1 - \xi + \xi^2 + \xi^3) \tag{3.15}$$

Alternatively we can write these as

$$u = \mathbf{P}^T(\xi)\mathbf{a} \qquad u' = \mathbf{P_1}^T(\xi)\mathbf{a} \tag{3.16}$$

$$v = \mathbf{Q}^T(\xi)\mathbf{a} \qquad v' = \mathbf{Q_1}^T(\xi)\mathbf{a} \qquad v'' = \mathbf{Q_2}^T(\xi)\mathbf{a} \tag{3.17}$$

$$w = \mathbf{R}^T(\xi)\mathbf{a} \qquad w' = \mathbf{R_1}^T(\xi)\mathbf{a} \qquad w'' = \mathbf{R_2}^T(\xi)\mathbf{a} \tag{3.18}$$

$$\theta = \mathbf{S}^T(\xi)\mathbf{a} \qquad \theta' = \mathbf{S_1}^T(\xi)\mathbf{a} \qquad \theta'' = \mathbf{S_2}^T(\xi)\mathbf{a} \tag{3.19}$$

where single primes denote first derivatives with respect to x and double primes denote second derivatives with respect to x. $\mathbf{P}, \mathbf{Q}, \mathbf{R}, \mathbf{S}, \mathbf{P_1}, \mathbf{Q_1} \ldots$ etc. are vectors as given below

$$\mathbf{P}^T = \{N_1, N_2, 0, 0, 0, 0, 0, 0, N_3, N_4, 0, 0, 0, 0, 0, 0\} \tag{3.20}$$

$$\mathbf{P_1}^T = \{N_1', N_2', 0, 0, 0, 0, 0, 0, N_3', N_4', 0, 0, 0, 0, 0, 0\} \tag{3.21}$$

$$\mathbf{Q}^T = \{0, 0, N_1, N_2, 0, 0, 0, 0, 0, 0, N_3, N_4, 0, 0, 0, 0\} \tag{3.22}$$

$$\mathbf{Q_1}^T = \{0,0,N_1',N_2',0,0,0,0,0,0,N_3',N_4',0,0,0,0\} \quad (3.23)$$

$$\mathbf{Q_2}^T = \{0,0,N_1'',N_2'',0,0,0,0,0,0,N_3'',N_4'',0,0,0,0\} \quad (3.24)$$

...etc.

where N_1, N_2, N_3, N_4 are as given earlier and N_1', N_2', N_3', N_4' are the first derivatives and $N_1'', N_2'', N_3'', N_4''$ are the second derivatives with respect to x.

3.4 Virtual Work Equations

From Eq.(2.7), the strain can now be written in the following form

$$\begin{aligned}\varepsilon &= [\mathbf{P_1}^T - y\mathbf{Q_2}^T + yz\mathbf{S_2}^T - z\mathbf{R_2}^T]\mathbf{a} \\ &\quad + \frac{1}{2}\mathbf{a}^T[(\mathbf{Q_1} - z\mathbf{S_1})(\mathbf{Q_1}^T - z\mathbf{S_1}^T) + (\mathbf{R_1} + y\mathbf{S_1})(\mathbf{R_1}^T + y\mathbf{S_1}^T)]\mathbf{a} \quad (3.25)\\ &= \mathbf{B_0}^T\mathbf{a} + \frac{1}{2}\mathbf{a}^T\mathbf{B_1}\mathbf{a} \quad (3.26)\end{aligned}$$

where

$$\mathbf{B_0} = \mathbf{P_1} - y\mathbf{Q_2} + yz\mathbf{S_2} - z\mathbf{R_2} \quad (3.27)$$

$$\mathbf{B_1} = (\mathbf{Q_1} - z\mathbf{S_1})(\mathbf{Q_1}^T - z\mathbf{S_1}^T) + (\mathbf{R_1} + y\mathbf{S_1})(\mathbf{R_1}^T + y\mathbf{S_1}^T) \quad (3.28)$$

$\mathbf{B_0}$ corresponds to the linear part of ε and $\mathbf{B_1}$ to the nonlinear.

Applying a virtual displacement $\delta\mathbf{a}$, as $\mathbf{a} \rightarrow \mathbf{a} + \lambda\delta\mathbf{a}$, the following can be obtained

$$\begin{aligned}\varepsilon(\lambda) &= \mathbf{B_0}^T(\mathbf{a} + \lambda\delta\mathbf{a}) + \frac{1}{2}(\mathbf{a}^T + \lambda\delta\mathbf{a}^T)\mathbf{B_1}(\mathbf{a} + \lambda\delta\mathbf{a}) \\ &= \mathbf{B_0}^T\mathbf{a} + \lambda\mathbf{B_0}^T\delta\mathbf{a} + \frac{1}{2}\mathbf{a}^T\mathbf{B_1}\mathbf{a} + \frac{\lambda}{2}\delta\mathbf{a}^T\mathbf{B_1}\mathbf{a} \\ &\quad + \frac{\lambda}{2}\mathbf{a}^T\mathbf{B_1}\delta\mathbf{a} + \frac{\lambda^2}{2}\delta\mathbf{a}^T\mathbf{B_1}\delta\mathbf{a}\end{aligned}$$

Thus the virtual strain can be written as

$$\begin{aligned}\delta\varepsilon = (\frac{d\varepsilon}{d\lambda})_{\lambda\rightarrow 0} &= \mathbf{B_0}^T\delta\mathbf{a} + \frac{1}{2}\delta\mathbf{a}^T\mathbf{B_1}\mathbf{a} + \frac{1}{2}\mathbf{a}^T\mathbf{B_1}\delta\mathbf{a} \\ &= \mathbf{B_0}^T\delta\mathbf{a} + \frac{1}{2}\mathbf{a}^T\mathbf{B_1}^T\delta\mathbf{a} + \frac{1}{2}\mathbf{a}^T\mathbf{B_1}\delta\mathbf{a}\end{aligned}$$

$$
\begin{aligned}
&= (\mathbf{B_0}^T + \frac{1}{2}\mathbf{a}^T\mathbf{B_1} + \frac{1}{2}\mathbf{a}^T\mathbf{B_1}^T)\delta\mathbf{a} \\
&= (\mathbf{B_0}^T + \mathbf{a}^T(\frac{\mathbf{B_1} + \mathbf{B_1}^T}{2}))\delta\mathbf{a} \qquad (3.29)
\end{aligned}
$$

and since $\mathbf{B_1}$ is symmetrical (refer Eq. 3.28) i.e. $\mathbf{B_1} = \mathbf{B_1}^T$, Eq.(3.29) can be written as

$$\delta\varepsilon = (\mathbf{B_0}^T + \mathbf{a}^T\mathbf{B_1})\delta\mathbf{a} \qquad (3.30)$$

The stress σ can be written as (from Eq. 2.16)

$$\sigma = E(\mathbf{B_0}^T + \frac{1}{2}\mathbf{a}^T\mathbf{B_1})\mathbf{a} + G(\varepsilon) \qquad (3.31)$$

where

$$G(\varepsilon) = -[E\varepsilon - \{-|p_0| - m_1 E\varepsilon\}(1 - e^{\frac{E}{|p_0|}\varepsilon}](1 - \Delta(\varepsilon)) \qquad (3.32)$$

$d\sigma$ can be written as

$$d\sigma = E(\mathbf{B_0}^T + \mathbf{a}^T\mathbf{B_1})\delta\mathbf{a} + H(\varepsilon)(\mathbf{B_0}^T + \mathbf{a}^T\mathbf{B_1})\delta\mathbf{a} \qquad (3.33)$$

where

$$
\begin{aligned}
H(\varepsilon) &= \frac{dG(\varepsilon)}{d\varepsilon} \\
&= (-E - m_1 E(1 - e^{\frac{E}{|p_0|}(\varepsilon-\varepsilon_0)}) \\
&\quad -(-|p_0| - m_1 E(\varepsilon - \varepsilon_0))\frac{E}{|p_0|}e^{\frac{E}{|p_0|}(\varepsilon-\varepsilon_0)} \qquad (3.34)
\end{aligned}
$$

Hence the virtual work equation can be written as

$$\int_V \delta\varepsilon^T \sigma dV - \int_S \delta\mathbf{a}^T\mathbf{F}dS = 0$$

or

$$\int_V \delta\mathbf{a}^T(\mathbf{B_0} + \mathbf{B_1}\mathbf{a})\sigma dV - \int_S \delta\mathbf{a}^T\mathbf{F}dS = 0 \qquad (3.35)$$

Since this must hold for any $\delta\mathbf{a}$,

$$\int_V (\mathbf{B_0} + \mathbf{B_1}\mathbf{a})\sigma dV - \int_S \mathbf{F}dS = 0 \qquad (3.36)$$

Thus we can write a function $\psi(\mathbf{a})$ as

$$\psi(\mathbf{a}) = \int_V (\mathbf{B_0} + \mathbf{B_1 a})\sigma dV - \int_S \mathbf{F} dS \tag{3.37}$$

The solution vector $\mathbf{a}$ must satisfy $\psi(\mathbf{a}) = 0$. To find this solution an iterative procedure is used. The Newton-Raphson method is a commonly used iterative technique to solve non-linear equations. It uses a truncated Taylor series expansion of the function $\psi(\mathbf{a})$

$$\psi(\mathbf{a} + \Delta\mathbf{a}) = \psi(\mathbf{a}) + [\frac{d\psi(\mathbf{a})}{d\mathbf{a}}]\Delta\mathbf{a} \tag{3.38}$$

or

$$\Delta\mathbf{a} = \psi(\mathbf{a} + \Delta\mathbf{a}) - \psi(\mathbf{a})[\frac{d\psi(\mathbf{a})}{d\mathbf{a}}]^{-1} \tag{3.39}$$

Setting $\psi(\mathbf{a} + \Delta\mathbf{a}) = 0$,

$$\Delta\mathbf{a} = \mathbf{a}_{i+1} - \mathbf{a}_i = -[\frac{d\psi(\mathbf{a})}{d\mathbf{a}}]^{-1}\psi(\mathbf{a_i}) \tag{3.40}$$

or

$$\mathbf{a}_{i+1} = \mathbf{a}_i - [\mathbf{K}_T]^{-1}\psi(\mathbf{a}_i) \tag{3.41}$$

Since

$$\begin{aligned} \delta\psi(\mathbf{a}) &= \int_V \mathbf{B_1}\delta\mathbf{a}\sigma dV + \int_V (\mathbf{B}_0 + \mathbf{B_1 a})\delta\sigma dV \\ &= \int_V \sigma\mathbf{B_1}\delta\mathbf{a} + \int_V [(\mathbf{B_0} + \mathbf{B_1 a})(E + H(\varepsilon)](\mathbf{B_0}^T + \mathbf{a}^T\mathbf{B_1})\delta\mathbf{a} \end{aligned} \tag{3.42}$$

Hence the tangent stiffness matrix can be written as

$$\begin{aligned} [\mathbf{K_T}] = \int_V [&\mathbf{B_1}E\mathbf{B_0}^T\mathbf{a} + \frac{1}{2}\mathbf{B_1}E\mathbf{a}^T\mathbf{B_1}\mathbf{a} + \mathbf{B_0}E\mathbf{B_0}^T + \mathbf{B_0}E\mathbf{a}^T\mathbf{B_1} \\ &+\mathbf{B_1 a}E\mathbf{B_0}^T + \mathbf{B_1 a}E\mathbf{a}^T\mathbf{B_1} + \mathbf{B_0}\mathrm{H}(\epsilon)\mathbf{B_0}^T + \mathbf{B_0}H(\epsilon)\mathbf{a}^T\mathbf{B_1} \\ &+\mathbf{B_1 a}H(\epsilon)\mathbf{B_0}^T + \mathbf{B_1 a}H(\epsilon)\mathbf{a}^T\mathbf{B_1} + \mathbf{B_1}G(\epsilon)]dV \end{aligned} \tag{3.43}$$

This tangent stiffness matrix is computed for each window and summed over the layers to find the element stiffness matrix. These are then assembled to obtain the global stiffness matrix.

Each value in the incremental solution vector $\Delta\mathbf{a}$ is compared against an acceptable tolerance specified by the user and it is determined whether further iteration is needed to obtain a sufficiently accurate solution vector $\mathbf{a}$.

3.5 Method of Computation

The Cholesky decomposition method is used in this program to invert the global stiffness matrix $[\mathbf{K}_{GT}]$ and to determine the solution displacement vector $\mathbf{a}$. The symmetrical and the banded character of the tangent stiffness matrix is utilised and only the band in the lower triange of the matrix is computed. After entering the boundary conditions, the $[\mathbf{K}_T]$ matrix is decomposed and the incremental solution displacement vector $\Delta\mathbf{a}$ is obtained using the residual load vector $\psi(\mathbf{a}_i)$. A flowchart for the computation is given in Fig. 3.3.

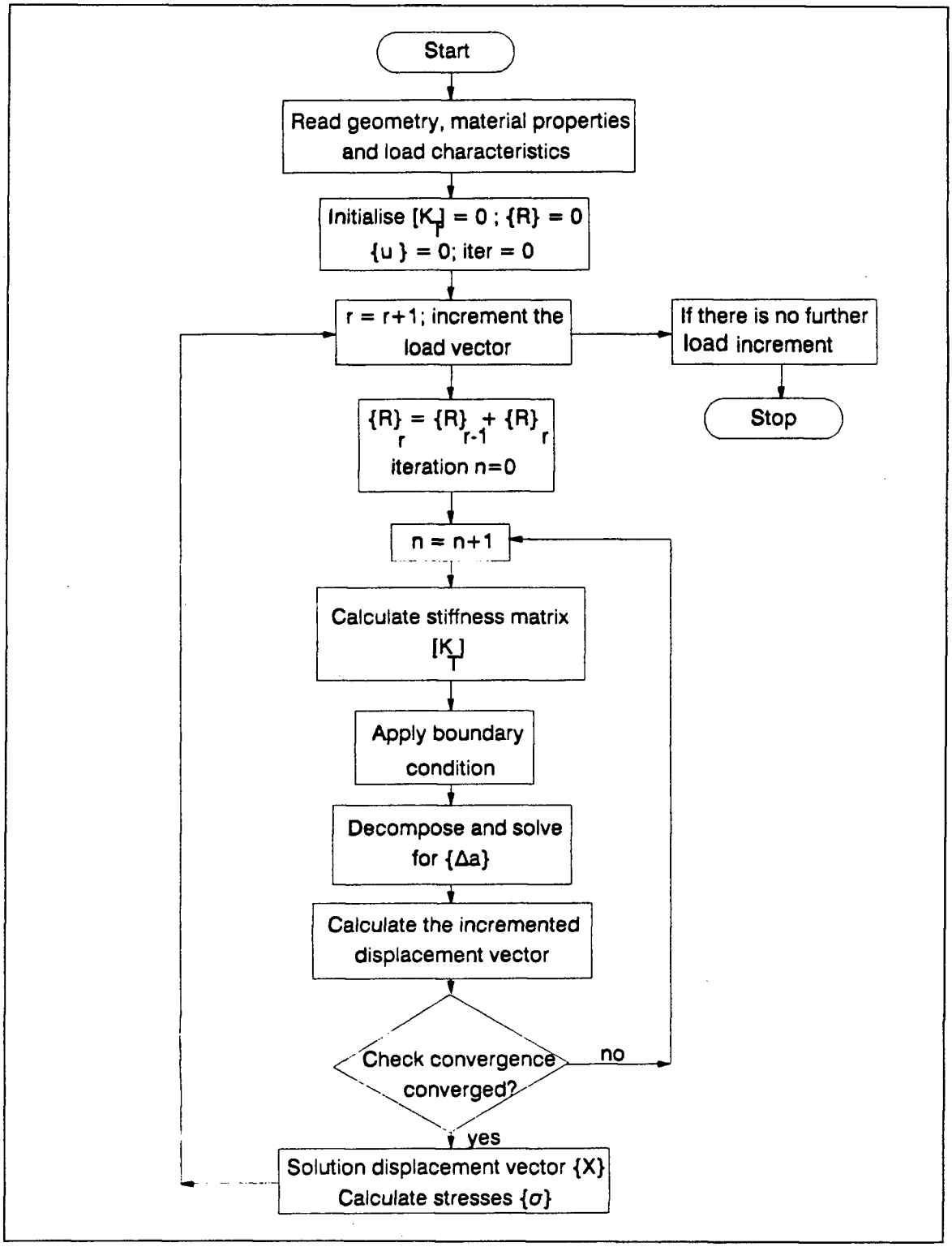

Figure 3.3: Flowchart for iterative technique using Newton-Raphson Method

3.6 Numerical Integration

Recourse must be made to numerical integration methods to obtain the matrix $[\mathbf{K}_T]$. Gauss quadrature allows the integral I to be computed as

$$I = \int_{-1}^{1} f(\xi)d\xi = \sum_{1}^{n} H_i f(\xi_i) \tag{3.44}$$

where ξ_i are fixed abscissae and H_i corresponding weights for the n chosen integration points. If a polynomial expression is to be integrated, it is easy to see that for n sampling points, there are $2n$ unknowns (H_i and ξ_i) and hence a polynomial of degree $(2n-1)$ could be constructed and exactly integrated. The error thus is of the order of $O(\Delta^{2n})$. In the present problem, since there are terms involving x, y and z, a Gaussian integration scheme is employed, which is of the form

$$\begin{aligned} I &= \int_{-1}^{1}\int_{-1}^{1}\int_{-1}^{1} f(\xi,\eta,\zeta)d\xi d\eta d\zeta \\ &= \sum_{k=1}^{n1}\sum_{j=1}^{n2}\sum_{i=1}^{n3} H_i H_j H_k f(\xi_i,\eta_j,\zeta_k) \end{aligned} \tag{3.45}$$

where $n1, n2, n3$ are number of integration points in x, y and z directions respectively. In the present case the integral I is of the form

$$I = \int_0^{\Delta w}\int_{-\frac{B}{2}}^{\frac{B}{2}}\int_0^{T} f(x,y,z)dxdydz \tag{3.46}$$

$$= \frac{\Delta w}{2}\frac{B}{2}\frac{T}{2}\int_{-1}^{1}\int_{-1}^{1}\int_{-1}^{1} f(\xi,\eta,\zeta)d\xi d\eta d\zeta \tag{3.47}$$

$$= \frac{\Delta w}{2}\frac{B}{2}\frac{T}{2}\sum_{k=1}^{n1}\sum_{j=1}^{n2}\sum_{i=1}^{n3} H_i H_j H_k f(\xi_i,\eta_j,\zeta_k) \tag{3.48}$$

where Δw is the length, B the width and T the thickness of each window.

As was pointed out earlier, n Gauss points integrate a polynomial of the order $(2n-1)$ exactly. In the stiffness expression in Eq. 3.43, there is a polynomial of order 8 in the $x-$direction, of order 4 each in $y-$ and $z-$directions. Hence a 5-point Gaussian integration in x-direction and a 3-point Gaussian integration in y- and z-directions are needed respectively. However it is important to note that in the program FENMBC

there is a flexibility of choosing the number of Gauss points from 1 to 5. This has been done because the program can handle multilayered beam columns and a number of windows within an element, to take care of the continuous variation of material properties along the span.

For example, if there is a beam column with 8 layers and 5 windows per element, one Gauss point in both x- and z-directions would give fairly accurate results as shown later. Also depending on the orientation of the loading the number of Gauss points in y- and z-directions should be suitably selected. For example if there is a distributed load in the z-direction on a beam column with only one layer, three Gauss points in z-direction and one Gauss point in y-direction would give accurate results. However if the applied load is acting in the y-direction then three Gauss points in y-direction and one Gauss point in z-direction would suffice. In case of biaxial loading, sufficient number of Gauss points should be chosen in both y- and z-directions. Thus one has to be careful in choosing the number of Gauss points in various directions.

Finally it should be mentioned that since numerical integration has been employed, stresses and strains can be determined only at the Gaussian points. If stresses and strains are needed at other points, a suitable interpolation may be employed.

3.7 Convergence Criterion

An Euclidean norm criterion has been used to check the convergence at every load step. If $\vec{a}_r$ is the solution vector at the end of r^{th} iteration and $\vec{a}_{r+1}$ is the solution at the end of $(r+1)^{th}$ iteration in Fig. 3.4, then $\Delta x = |\vec{a}_{r+1} - \vec{a}_r|$ represents the difference between the two displacement vectors. $|\vec{a}_r|$ and $|\vec{a}_{r+1}|$ can be given as follows

$$|\vec{a}_r|^2 = \sum_{i=1}^{NDOF} a_r^2(i)$$

$$|\vec{a}_{r+1}|^2 = \sum_{i=1}^{NDOF} a_{r+1}^2(i)$$

where $a_r(i)$ and $a_{r+1}(i)$ are components of $\vec{a}_r$ and $\vec{a}_{r+1}$ respectively.

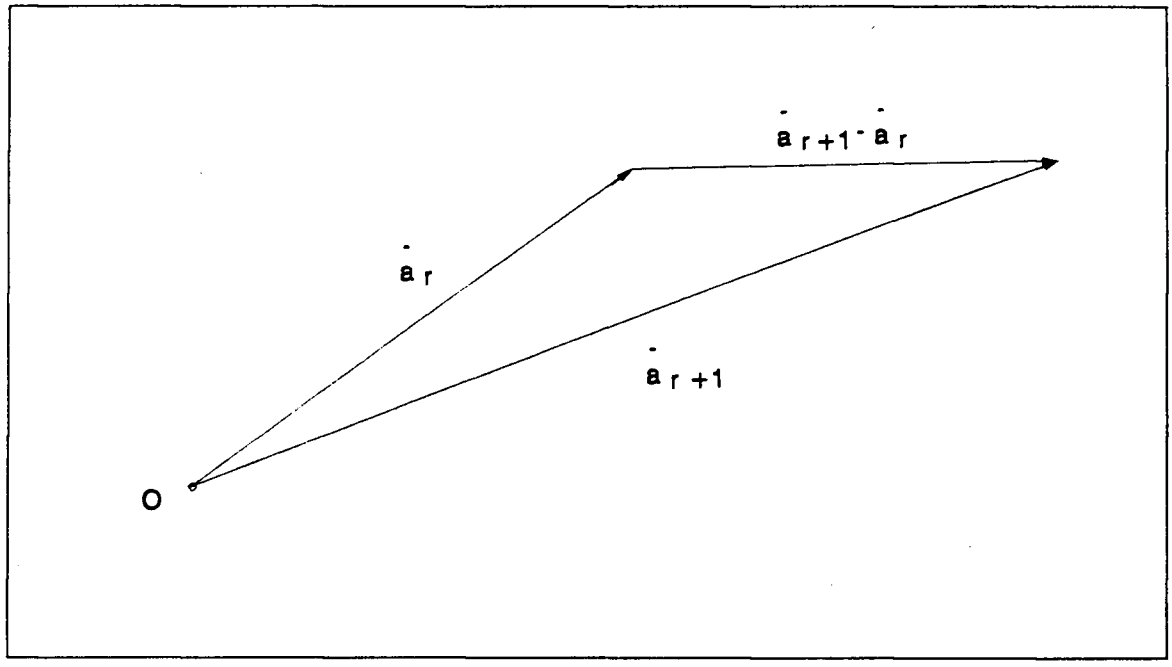

Figure 3.4: Convergence criterion

Then Δa can be written as

$$\Delta a = \sum_{i=1}^{NDOF} \sqrt{(a_{r+1}(i) - a_r(i))^2} \tag{3.49}$$

The convergence criterion for this norm is given as

$$\frac{\Delta a}{|\vec{a}_r|} \leq specified\ tolerance \tag{3.50}$$

3.8 FENMBC—the Computer Program

A computer program called FENMBC (Finite Element Nonlinear analysis of Multilayered Beam Column) based on the above finite element formulation was developed. It is a versatile finite element program capable of analyzing a 3-dimensional multilayered beam-columns with numerous possibilities in terms of geometric, material properties and loading conditions. Extensive numerical testing was done and some of the results have been reported in the next chapter.

CHAPTER 4

Verification and Numerical Results

Numerical results obtained from FENMBC were compared with analytical, experimental or numerical results published in the literature, whenever possible. The cases presented below involve geometric nonlinearity, material nonlinearity, biaxial bending, buckling, lateral stability and torsion. These cases have been tested for both single as well as multilayered beam-columns and the results are reported here.

The program FENMBC has been implemented and tested on a mainframe, Amdahl 5840, a Sun 4/260 workstation and an AST 286 Premium (IBM PC-AT compatible) at the University of British Columbia. Double Precision (`Real*8`) arithmetic is used throughout the program to reduce the effect of round-off.

The program has the capability of handling 20 layers, 20 elements and 10 windows per element. Each window can have a maximum of 5 Gauss points in the three principal axes directions. The dimensions in the program can be easily modified to accomodate a greater number of layers, elements, windows and Gauss points.

The large deflection results given by Timoshenko [25] for beam-bending were used to verify the program's numerical results.

4.1 Fixed Ended Beam Under Uniform Load

The numerical results for a fixed ended beam were obtained. The data for the beam have been given below.

Timoshenko used the energy method to obtain an approximate solution for a plate

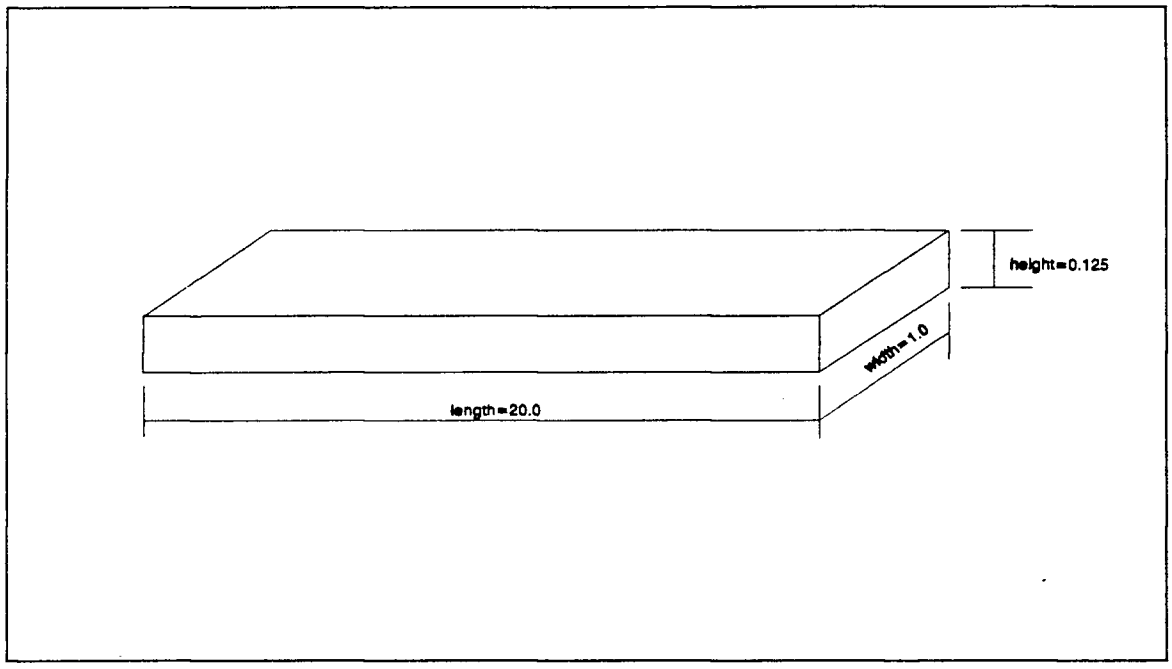

Figure 4.1: Data for Timoshenko's fixed ended beam bending problem

with fixed edges. He obtained the total strain energy of the plate by adding the energy due to bending and the energy due to the strain of the middle surface and then used the principle of virtual work. He used the following displacement functions satisfying the boundary conditions imposed by the clamped edges for a rectangular plate with sides $2a$ and $2b$.

$$u = (a^2 - x^2)(b^2 - y^2)x(b_{00} + b_{02}y^2 + b_{20}x^2 + b_{22}x^2y^2) \tag{4.1}$$

$$v = (a^2 - x^2)(b^2 - y^2)y(c_{00} + c_{02}y^2 + c_{20}x^2 + c_{22}x^2y^2) \tag{4.2}$$

$$w = (a^2 - x^2)^2(b^2 - y^2)^2(a_{00} + a_{02}y^2 + a_{20}x^2) \tag{4.3}$$

The values of all the parameters were estimated for various intensities of the load q and for different aspect ratios $\frac{a}{b}$, assuming $\nu = 0.3$. The results reported for an infinitely long plate (for $\frac{a}{b} = 0$) have been used to compare with the results of FENMBC.

4.1.1 Finite Element Results

The program FENMBC was run using the data shown above with some additional data required for the program: number of layers $nlayer = 1$, number of windows $nwindo = 3$, number of Gauss points along span in x-direction $ngauss = 5$, number of Gauss points along the width in y-direction $ngausy = 2$, Number of Gauss points along the depth in z-direction $ngausz = 5$, slope of the compression curve $m_1 = 0.2$, and high values for maximum allowable tensile and compressive stresses of $F_c = 6.0 \times 10^{15} N/m^2$ and $F_t = 6.0 \times 10^{15} N/m^2$ to ensure full elastic behavior. The distributed load in the z-direction was given as $q_z = 10.7315 N/m$ and the number of load steps was specified as 16 for a smooth load-displacement relationship. The results have been tabulated in Table 4.1 and subsequently shown graphically in Fig. 4.2. The program FENMBC's results are in good agreement with Timoshenko's results.

In the Table 4.1, the theoretical linear, Timoshenko's nonlinear and FENMBC's nonlinear results have been presented. q is the uniformly distributed load, l is the span, $D = EI$, where E is modulus of elasticity and I is moment of inertia of the beam cross-section along y-axis, h is the depth of the beam and w_{max} is the maximum displacement in z- direction. From Table 4.1, It should be noted that the order of accuracy is quite good even with 6 elements as compared to 20 elements.

Table 4.1: Comparison of Timoshenko and FENMBC solution for large deflection of beams

$\frac{ql^4}{Dh}$	Linear theoretical $(\frac{w_{max}}{h})$	Timoshenko nonlinear $(\frac{w_{max}}{h})$	FENMBC nonlinear 6 elements $(\frac{w_{max}}{h})$	FENMBC nonlinear 10 elements $(\frac{w_{max}}{h})$	FENMBC nonlinear 20 elements $(\frac{w_{max}}{h})$
0.0	0.0	0.0	0.0	0.0	0.0
10.0	0.4166667	0.40	0.4081488	0.4082008	0.4082064
20.0	0.8333333	0.62	0.6828256	0.6832096	0.6832456
30.0	1.2500000	0.84	0.8791920	0.8798320	0.8799200
40.0	1.6666667	0.98	1.0311120	1.0321920	1.0323440
50.0	2.0833333	1.10	1.1571440	1.1586880	1.1589200
60.0	2.5000000	1.21	1.2654880	1.2675280	1.2678400
70.0	2.1966667	1.31	1.3610000	1.3635520	1.3639520
80.0	3.3333333	1.39	1.4467600	1.4498240	1.4503200
90.0	3.7500000	1.47	1.5248480	1.5284240	1.5290160
100.0	4.1666667	1.54	1.5967040	1.6007920	1.6014800
110.0	4.5833333	1.62	1.6634000	1.6680080	1.6688000
120.0	5.0000000	1.67	1.7257520	1.7308720	1.7317680
130.0	5.4166667	1.73	1.7861440	1.7917760	1.7927760
140.0	5.8333333	1.79	1.8413200	1.8474560	1.8485600
150.0	6.2500000	1.84	1.8937040	1.9003360	1.9015520
160.0	6.6666667	1.90	1.9436160	1.9507440	1.9520720

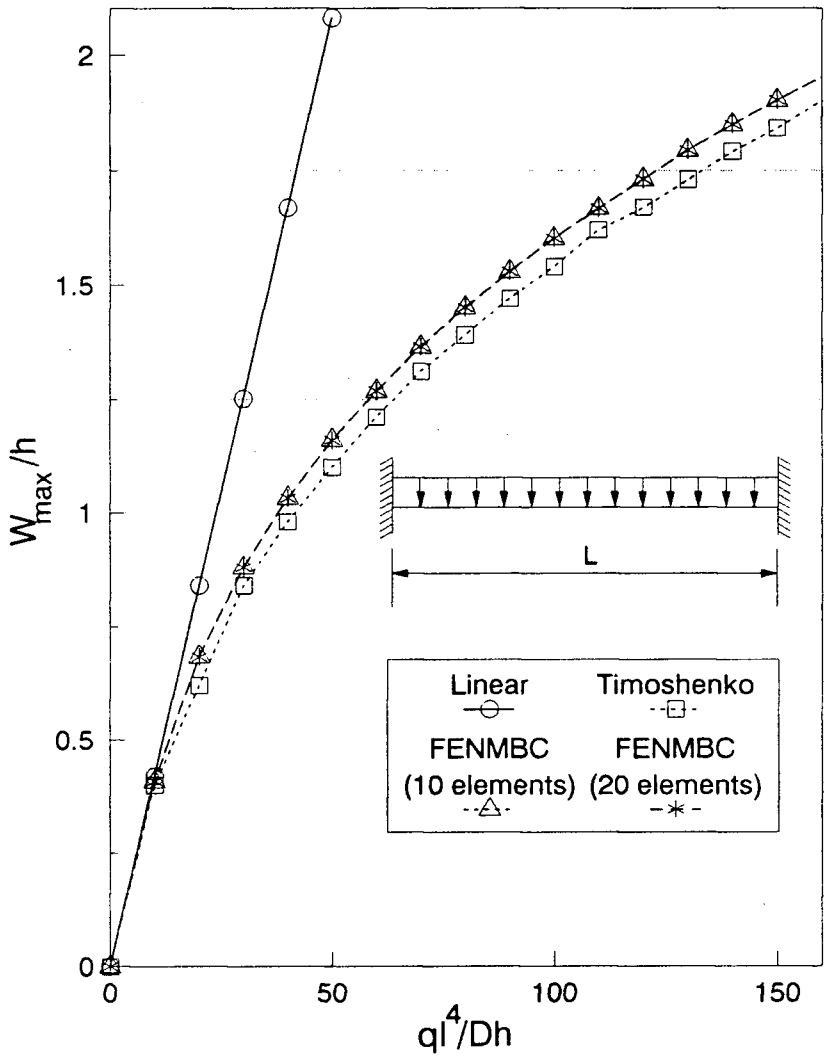

Figure 4.2: Comparison of Timoshenko's and FENMBC's large beam-bending

4.2 Other Test Cases

Other cases were run and the results have been reported below. These have been compared with the linear beam bending and beam column theories for lack of available nonlinear results. The same two data sets were used throughout the investigation unless otherwise specified. The first data set contained 10 layers with their elasticity moduli placed symmetrically with respect to the y-axis on the beam cross-section as shown in Fig. 4.3. The second data set contained 10 layers with their elasticity moduli placed asymmetrically with respect to the y-axis of the beam cross-section as shown in Fig. 4.3.

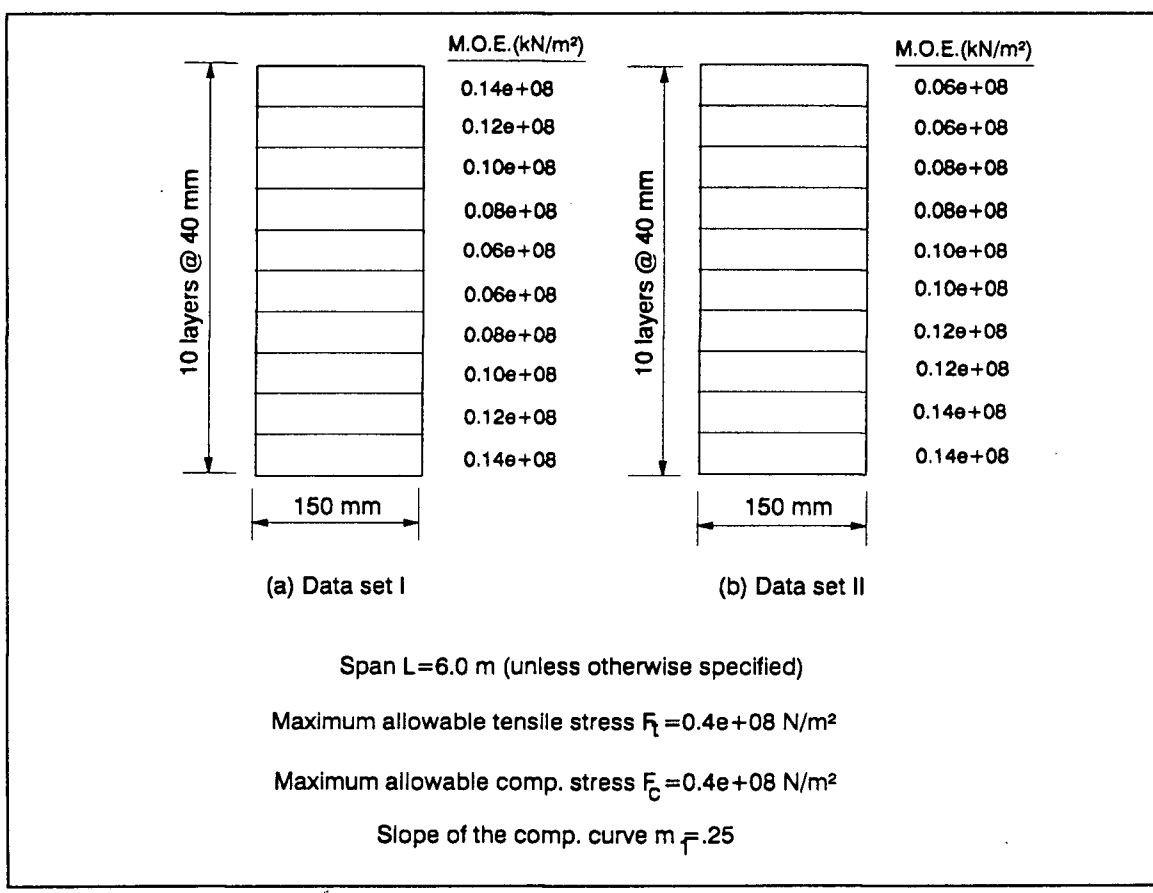

Figure 4.3: Data for the test cases

4.2.1 Simply Supported Multilayered Beam under Biaxial Loading for Data-set I

The case of a multilayered beam with data-set I as shown in Fig. 4.3 with concentrated loads in y- and z-directions (refer Fig. 4.4) was run. The additional data required for running FENMBC were: $nelem = 10, nwindo = 3, ngauss = 3, ngausy = 5, ngausz = 5$. The maximum tensile and compressive stress values was taken as $4.0 \times 10^{10} N/m^2$ for all the layers.The concentrated loads were $P_y = 1.0 \times 10^6 N \text{and} P_z = 1.0 \times 10^6 N$. The displacement results have been reported in Fig. 4.4. The total tensile stresses comprising of biaxial bending stresses and axial stresses at the Gauss point located at $nelem = 6, nlayer = 10, nwindo = 1, ngauss = 1, ngausy = 5, ngausz = 5$ has been shown in Fig. 4.5.

The linear deflections v and w were calculated from the linear beam bending theory using the method of transformed cross-section for comparison with the nonlinear results obtained from FENMBC. The nonlinear displacements v and w are the maximum displacements (at node no. 6) and are the same for all the layers. As both the ends are hinged, the displacements converge to a lower value from the linear displacement values due to stiffening of the beam resulting from the large deformation terms.

The rotation θ, as obtained in the result shown in Fig. 4.4, needs some explanation. For symmetric loading in biaxial bending of beam finite element model, one would usually expect displacements only in transverse and lateral directions. In the present case of biaxial bending of a simply supported rectangular multilayered beam, the support condition may be thought of as a knife-edge support. The loadings in transverse and lateral directions are applied incrementally. The load in y-direction, ΔP_y, produces a displacement Δv. As the first load increment ΔP_z is applied, there exists a moment $\Delta M_z = \Delta P_z \times \Delta v$, which causes a rotation in the beam cross-section along x-axis. Also the force ΔP_z produces the displacement Δw in z-direction. As

the loads are incremented gradually, the rotation also increses. In the mathematical formulation of the stiffness matrix given by the Eq. 3.43, the rotation comes from the coupled terms involving S_1 and S_2, these being the derivatives of the shape functions for θ. The odd terms in y and z after integration cancel out due to the symmetry of layers, however, the even terms add up and produce the desired rotational deformation. The total tensile stresses are seen to be linear as indeed they should be, since they are in the tensile zone below the maximum tensile stress F_T.

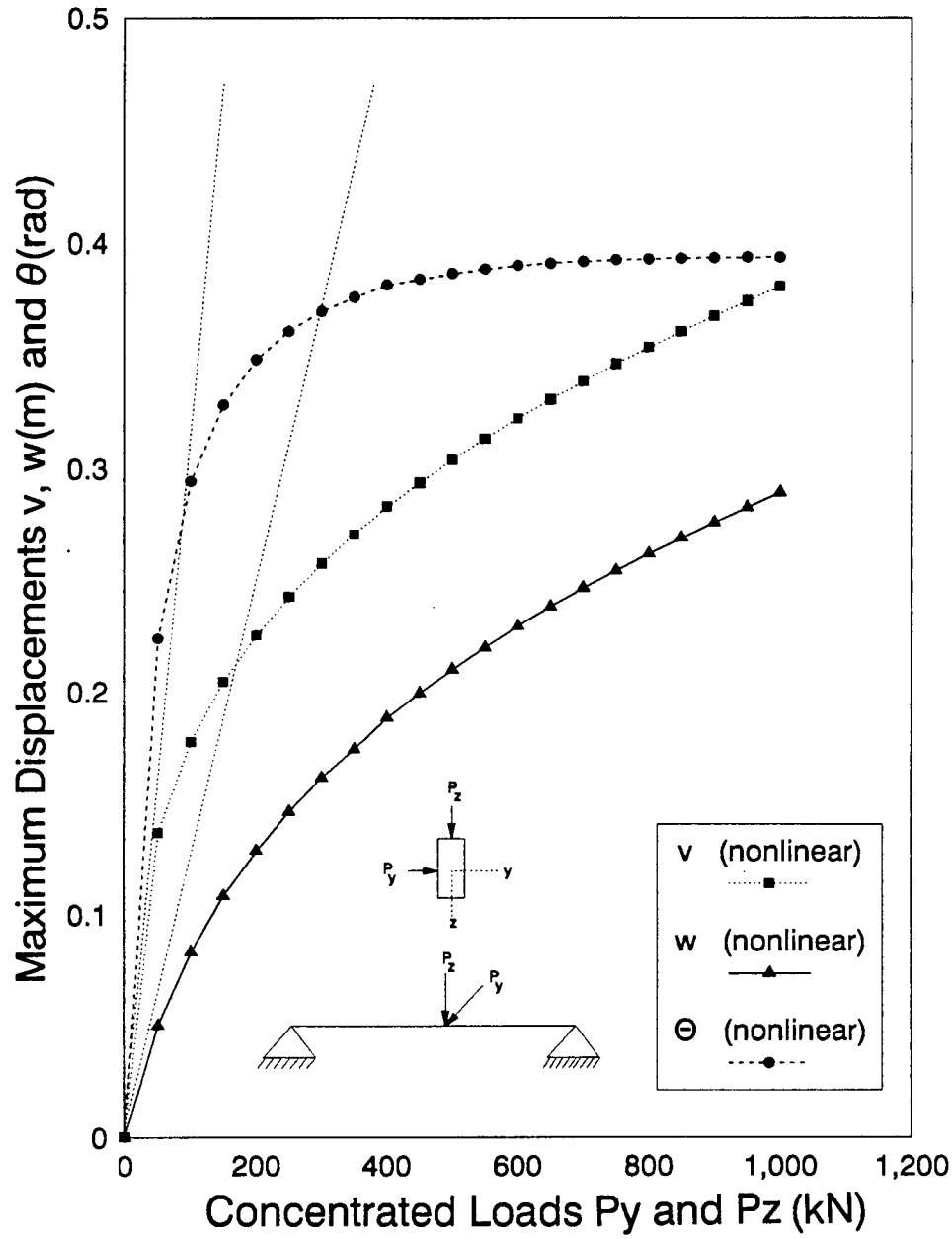

Figure 4.4: Displacement results for biaxially loaded multilayered beams for data-set I

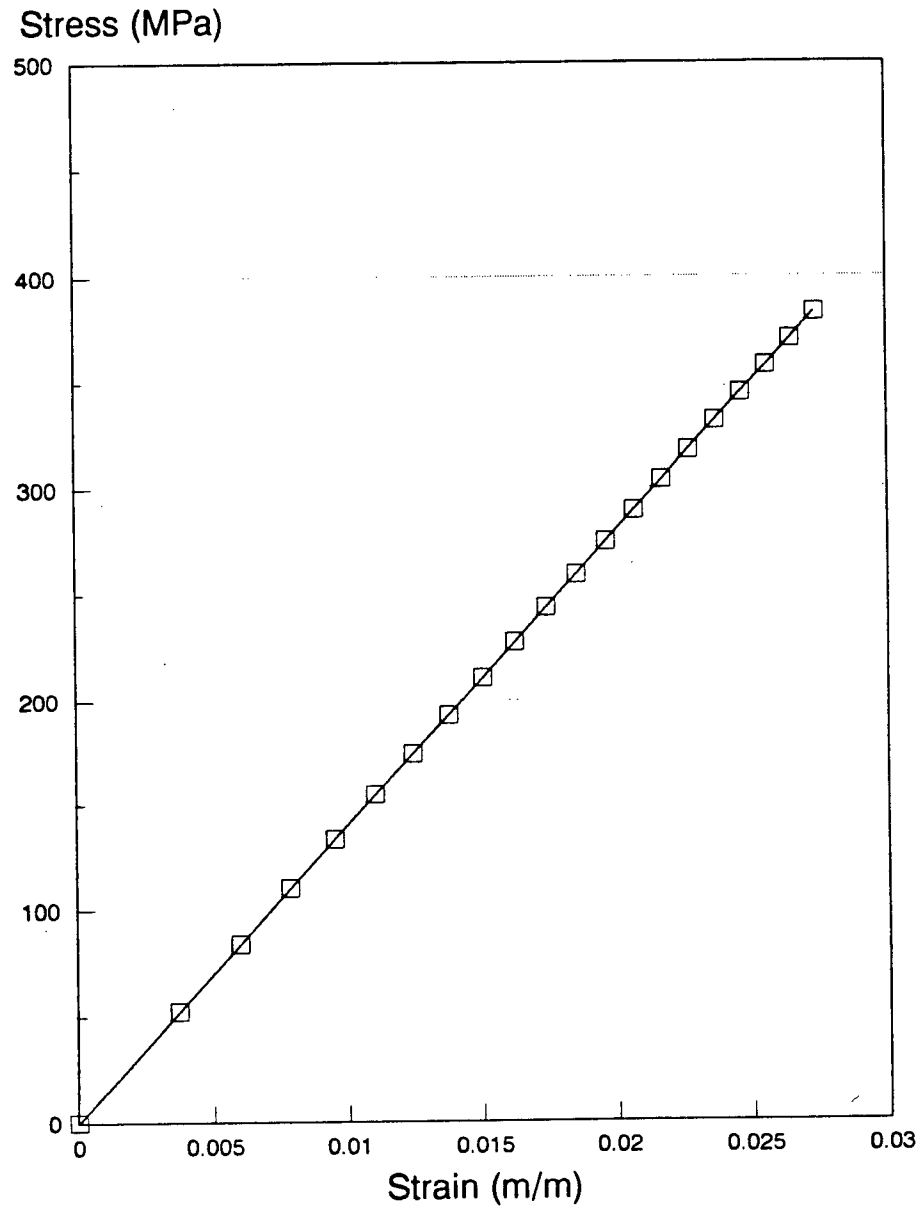

Figure 4.5: Stresses for biaxially loaded multilayered beams for data-set I

4.2.2 Simply Supported Multilayered Beam under Biaxial Loading for Data-set II

The other multilayered beam with data-set II as shown in Fig. 4.3 with concentrated loads in y- and z-directions (refer Fig. 4.6) was run. The additional data required for running FENMBC were: $nelem = 10, nwindo = 3, ngauss = 3, ngausy = 5, ngausz = 5$. The maximum tensile and compressive stress values was taken as $4.0 \times 10^{10} N/m^2$ for all the layers.The concentrated loads were $P_y = 1.0 \times 10^6 N \text{and} P_z = 1.0 \times 10^6 N$. The displacement results have been reported in Fig. 4.6. The total tensile stresses comprising of biaxial bending stresses and axial stresses at the Gauss point located at $nelem = 6, nlayer = 10, nwindo = 1, ngauss = 1, ngausy = 5, ngausz = 5$ has been shown in Fig. 4.7.

The linear deflections v and w were again calculated from the linear beam bending theory using equivalent cross-section. The transverse and lateral deflections resulting from the rotation θ were ignored in this calculation due to their small magnitude. The nonlinear displacements v and w again converge to a lower value from the linear displacement values as discussed earlier. The rotation θ in this case results from the torsional rigidity as explained in Section 4.2.1 as well as due to asymmetric placement of the beam layers in data-set II. The total tensile stresses are seen to be linear again, as they are in the tensile zone below the maximum tensile stress F_T.

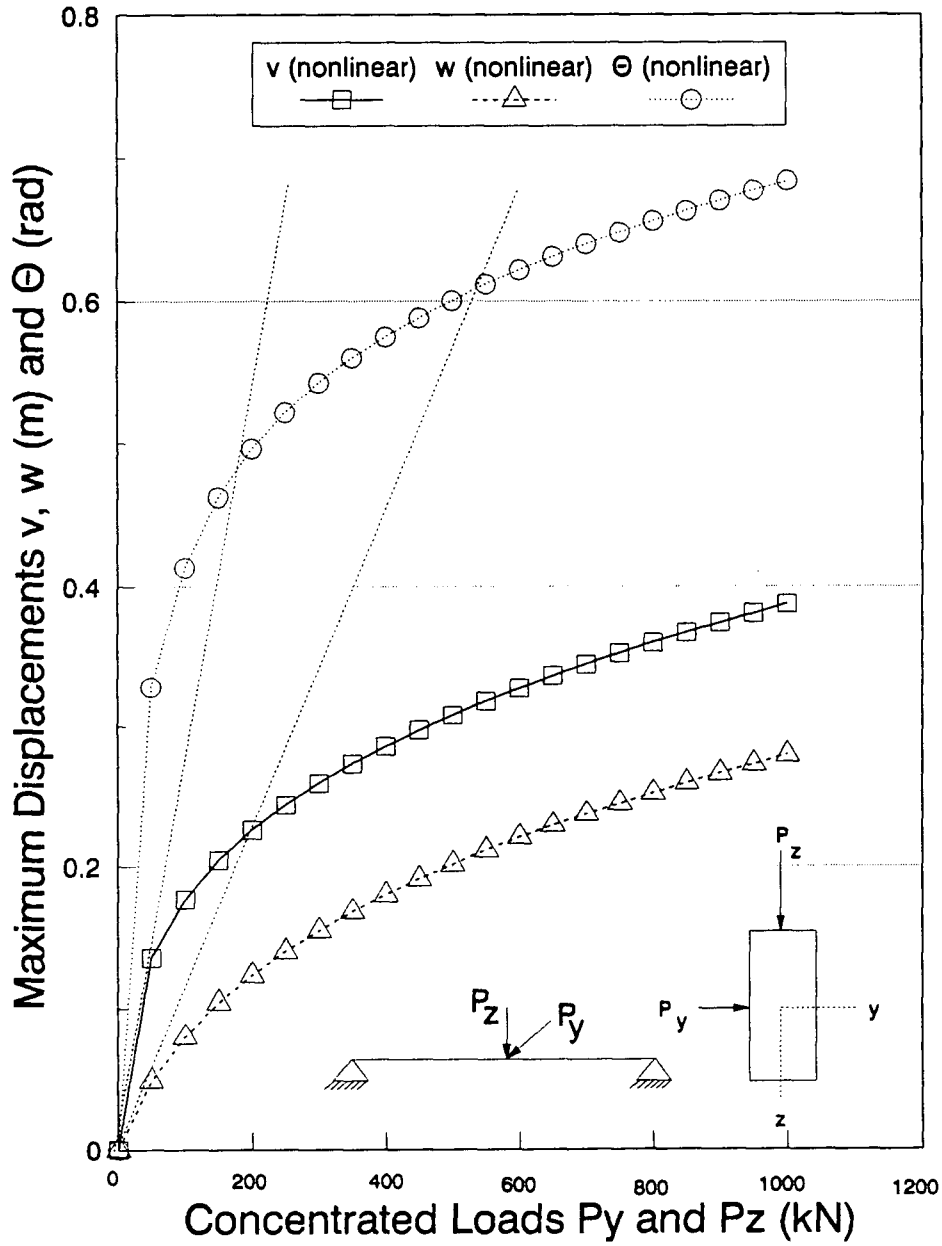

Figure 4.6: Displacement results for biaxially loaded multilayered beams for data-set II

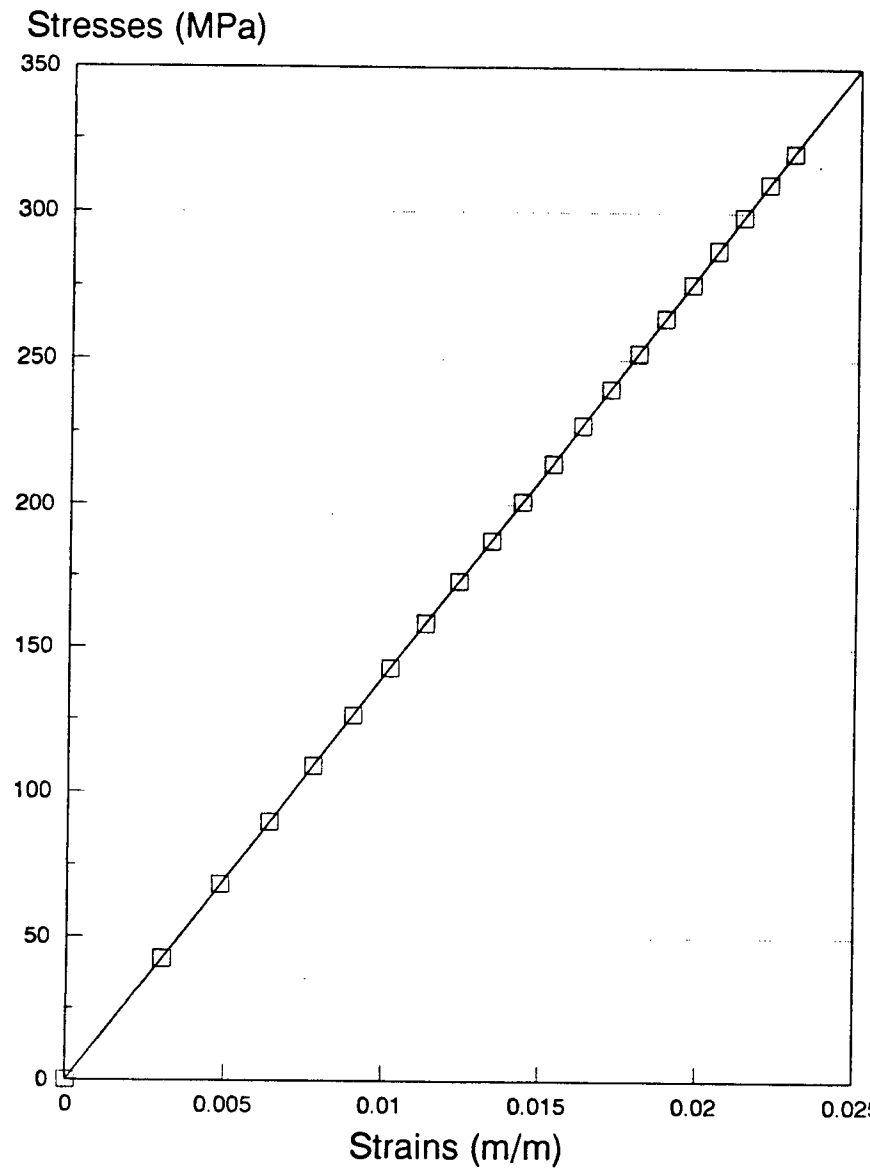

Figure 4.7: Stresses for biaxially loaded multilayered beams for data-set II

4.2.3 Eccentric biaxial loading on Simply Supported Beam for Data-set I

The multilayered beam with data-set I as shown in Fig. 4.3 with eccentrically located concentrated loads in y- and z-directions (refer Fig. 4.8) was run. The additional data required for running FENMBC were the same as in Section 4.2.1 with eccentricities $e_y = 20mm$ and $e_z = 20mm$. The displacement results have been reported in Fig. 4.8.

The nonlinear displacements v and w again converge to a lower value from the linear displacement values as expected. At the beginning the rotation θ is zero as are the loads applied. However as the first load increment is applied, θ takes on a negative value. As can be seen from the loading in the Fig. 4.8, the moments produced at the centroidal axis of the beam due to the two eccentric loadings are in opposite directions. Depending on the load magnitude, eccentricity and torsional rigidity, a negative rotation occurs on applying the first load increment. As the load is increased, the rotation also gets affected by the displacements v and w as explained in Section 4.2.1. The interaction of these moments produces the rotational deformations as shown in Fig. 4.8. The stress-strain diagram has not been included here as the tensile and compressive stresses are still in the linear elastic range. An example of nonlinear stress-strain behavior under biaxial loading has been discussed later in this chapter.

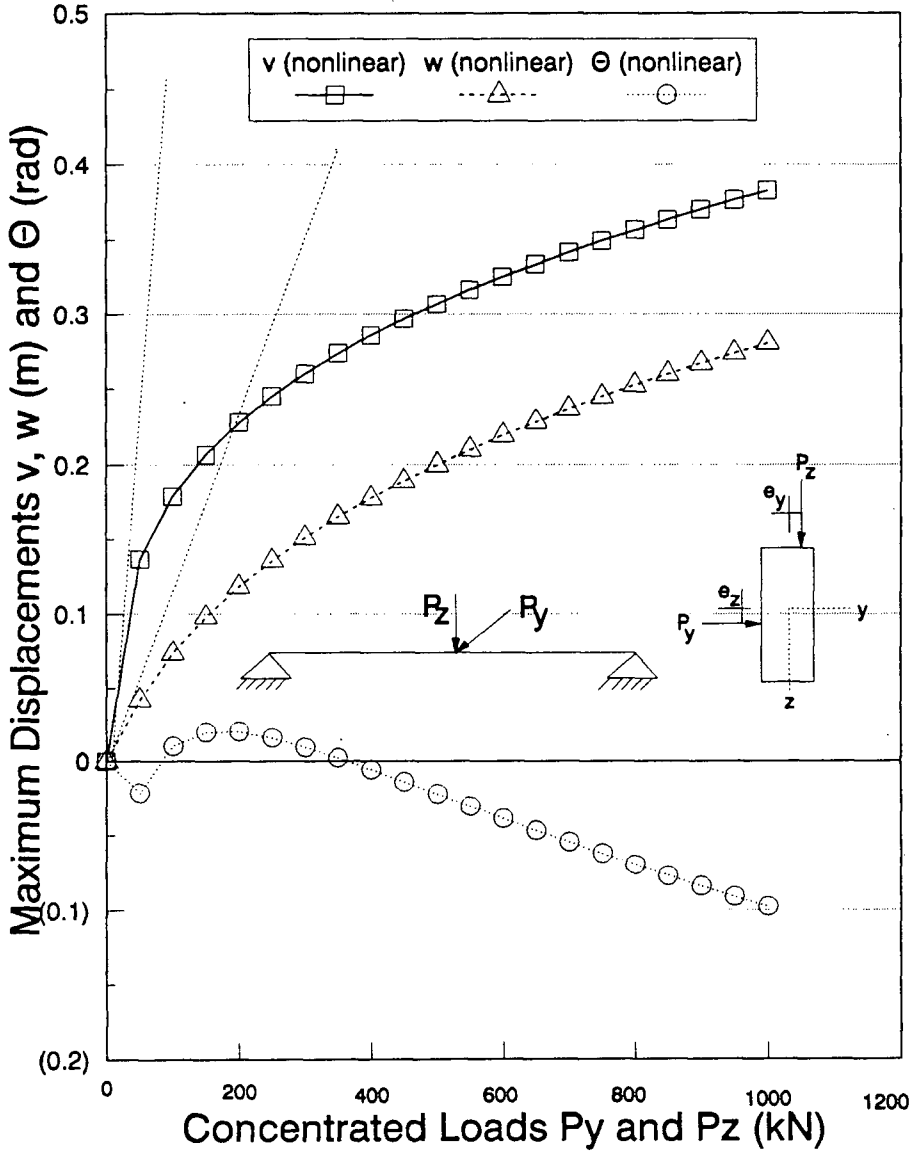

Figure 4.8: Displacement results for simply supported multilayered beams under eccentric biaxial loading for data-set I

4.2.4 Simply Supported Beam-Column with axial loading having eccentricity in y-direction for Data-set I

The program FENMBC was tested for buckling and the results were compared with Euler buckling loads for an equivalent cross-sectional area and a mean elasticity modulus E. The Euler buckling load thus calculated was $P_E = 173.49kN$. An axial load was applied with a very small eccentricity in the y-direction, and increased in steps of $8.6754kN$. As the load increases, the deflections become larger and finally the beam-column fails due to instability as it approaches the Euler buckling load. This demonstrates the program's capability to analyse beam-columns for buckling failures. The results have been reported in Fig. 4.9.

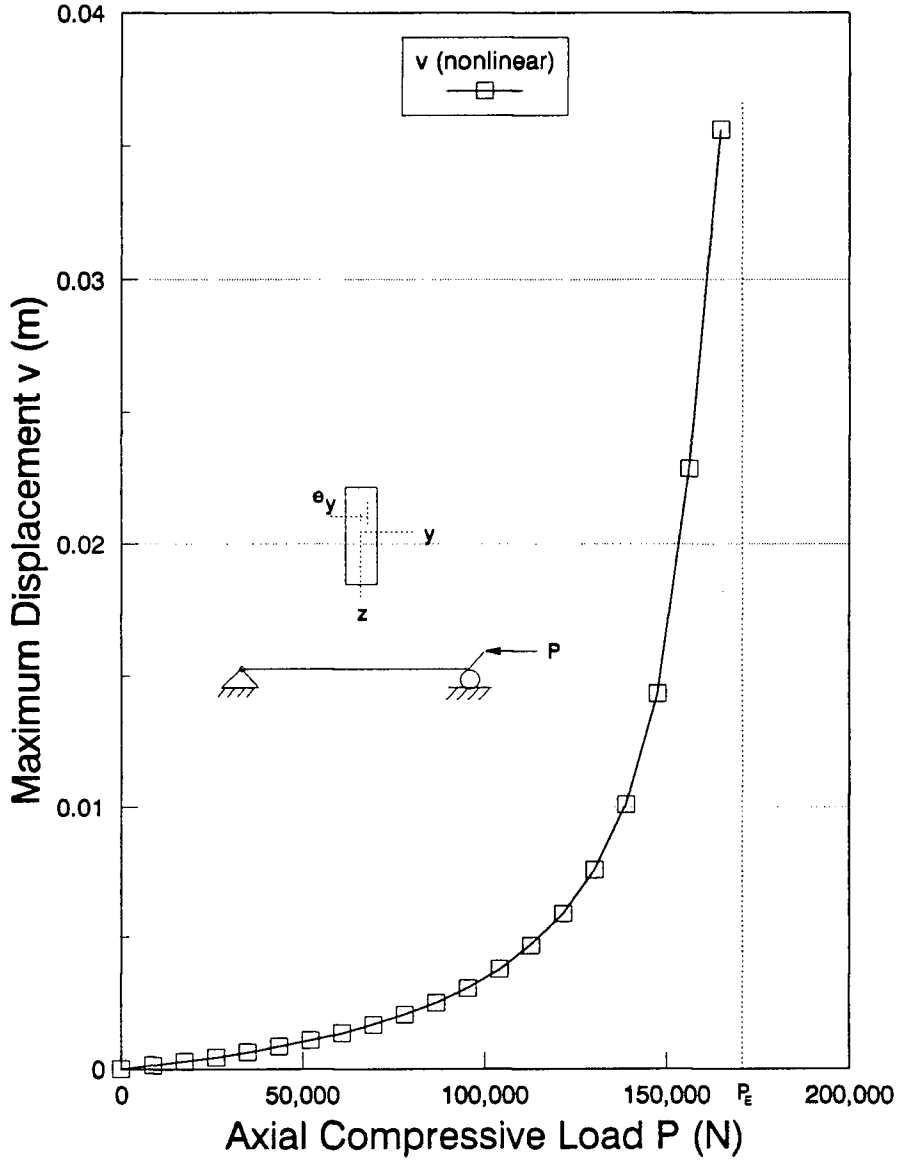

Figure 4.9: Displacement results for simply supported multilayered beam-column with axial loading having eccentricity in y-direction for data-set I

4.2.5 Simply Supported Beam-Column with axial loading having eccentricity in y-direction for Data-set II

The program FENMBC was further tested with data-set II for buckling and the results were compared with Euler buckling loads for an equivalent cross-sectional area and a mean elasticity modulus E. It should be noted, however, that the centroidal axis and the shear center axis do not coincide and the theoretical buckling load can be calculated using the transformed cross-section method. However, ignoring this fact, the Euler buckling load was calculated just to have an idea of the magnitude and was found to be $P_E = 173.49kN$ and was applied with a very small eccentricity in the y-direction. The results have been reported in Fig. 4.10.

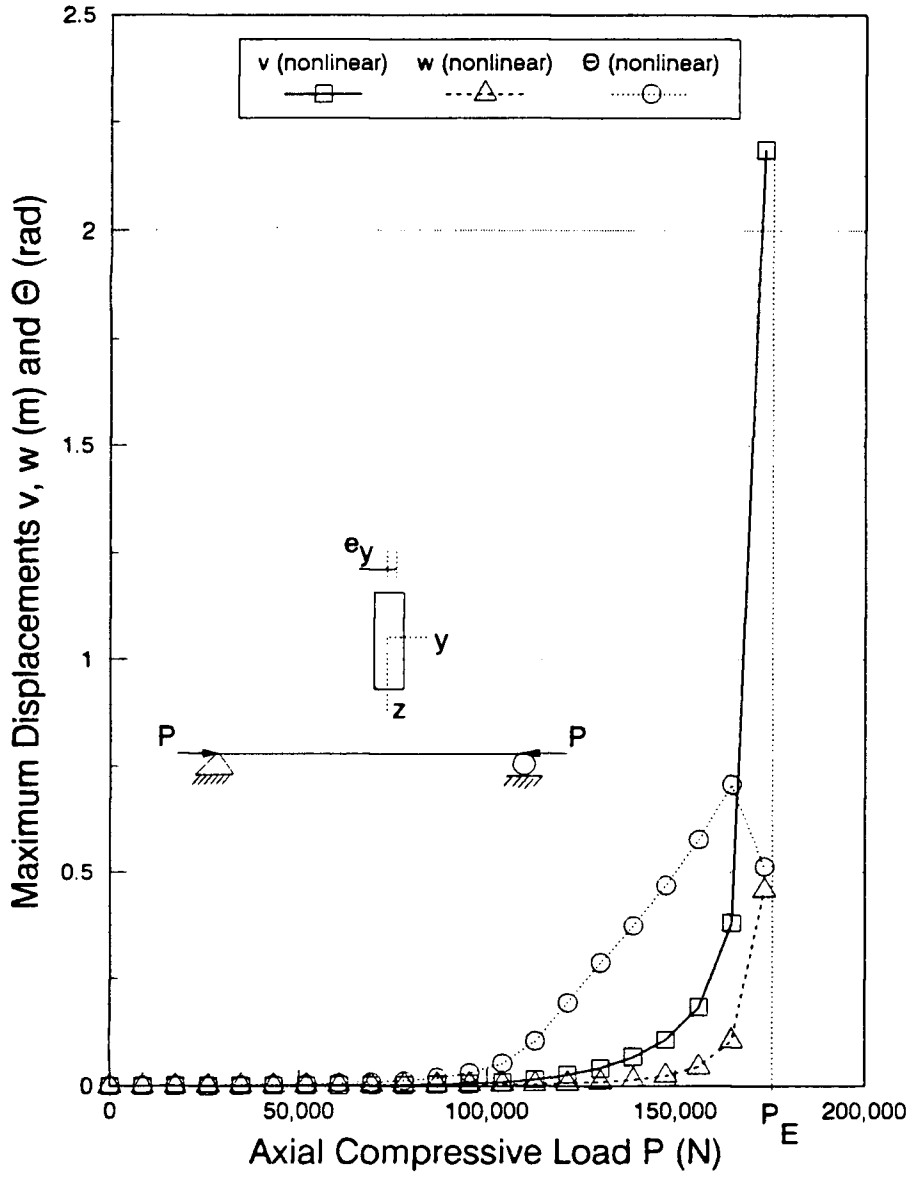

Figure 4.10: Displacement results for simply supported multilayered beam-column with axial loading having eccentricity in y-direction for data-set II

4.2.6 Simply Supported Multilayered Beam with a Nonlinear Compression Zone

The data-set I was used to test the response of the multilayered beam in the nonlinear compression zone. In the data-set I, the maximum allowable compressive stress values were divided by 100 to force the compressive stresses to fall in the nonlinear range. The loading and boundary conditions have been shown in Fig. 4.11 along with the deflections v and w. Once again the nonlinear deflections converge to lower values compared to the linear deflections due to the stiffening of the beam. This case was run to test the response of the multilayered beam in the nonlinear range. The stress-strain plot has been shown in the Fig. 4.12. Defining failure criteria for the beam-column in tensile as well as compression zone, the program can be used to predict member strengths and stability.

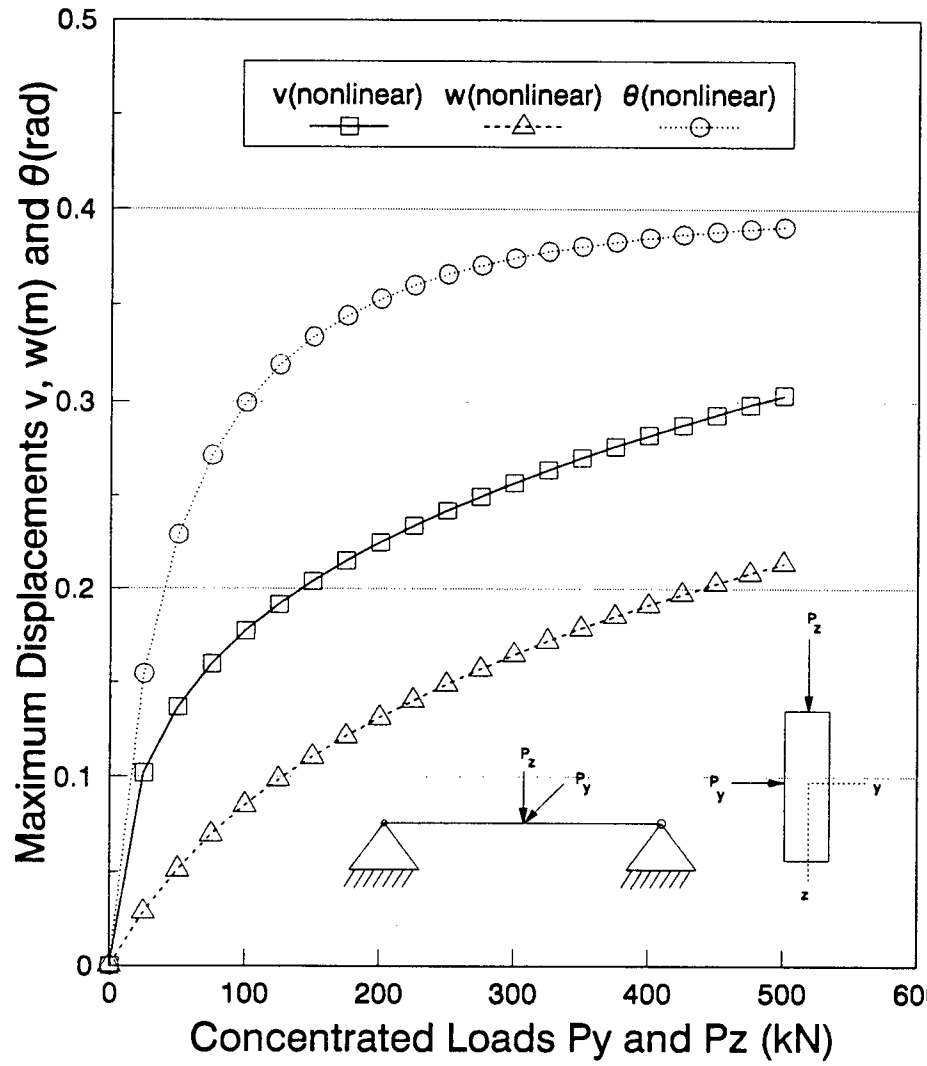

Figure 4.11: Displacement results for simply supported multilayered beams with a nonlinear compression zone

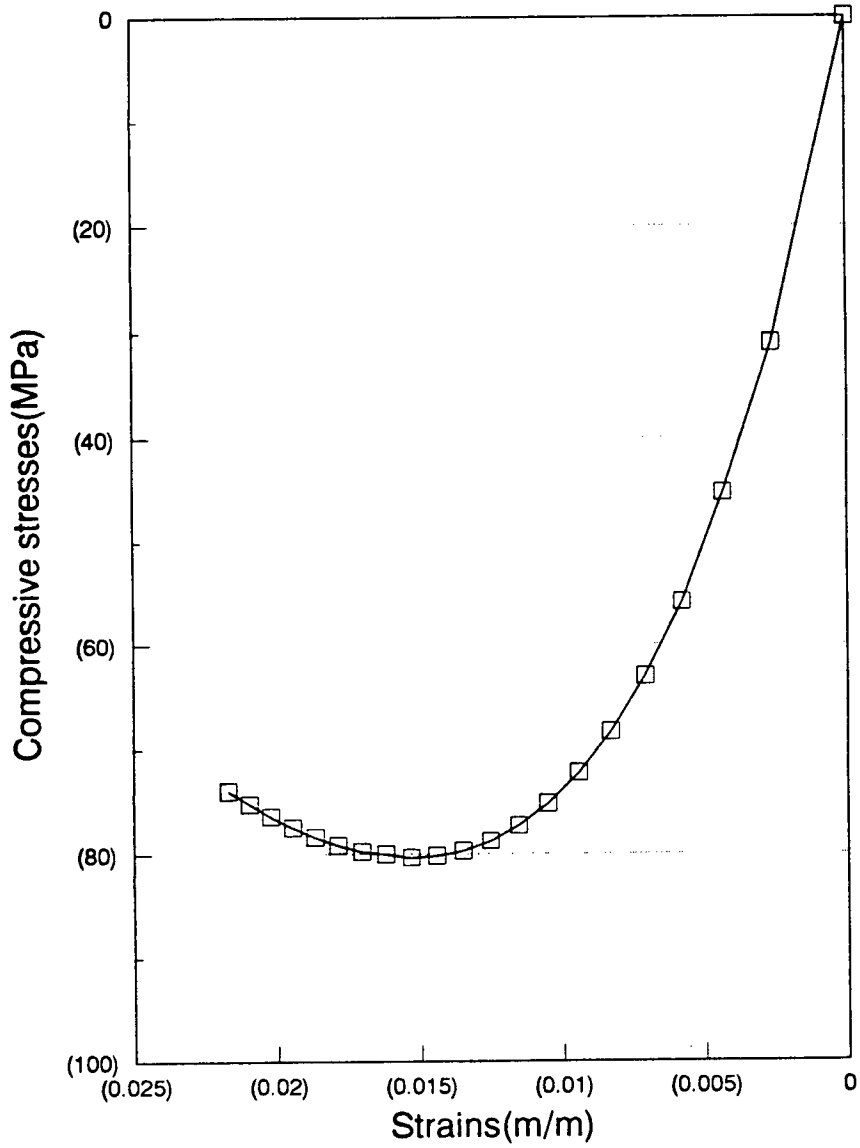

Figure 4.12: Stress-strain curve for simply supported multilayered beam with a non-linear compression zone

CHAPTER 5

Summary, Conclusions and Scope for Future Research

5.1 Summary and Conclusions

A direct virtual work formulation of multilayered beam-columns is developed incorporating geometric as well as material nonlinearities. Finite element total and incremental equilibrium equations are derived based on the assumed displacement model. This method has been used to examine the strength and stability of glued-laminated beam-columns. The computer program developed has been verified and tested for several beam-column problems. The generality of the model makes it a powerful and versatile tool for solving a large variety of problems.

The most important question for the user of the finite element method is whether the method yields sufficiently accurate results for his purpose. As conforming elements have been used for displacement functions satisfying completeness criteria, any desired degree of accuracy, with the limitations of finite element being an approximate method, could be obtained with suitably modifying the dimensions in the program. As in any other approximate numerical method, engineering judgement should be exercised in interpreting the results obtained by the finite element method since accuracy of the results depends on the assumptions employed in the formulation and the limitations of the material idealization.

Since the finite element model developed in the present study is quite general

in its application to glued-laminated beam-columns, it is now possible to carry out parametric studies for the codification of design procedures to include instability and effects of plastic members for realistic loading and material response.

5.2 Scope for Future Research

The present model does not include shear deformations in its formulation and hence it may not give very accurate results for short and stocky beam-columns. An inclusion of shear effects would enhance its capabilities.

A load path dependent plastic response of the material would make the model more realistic in terms of predicting long term behavior of the beam-column undergoing load reversals. An inclusion of creep behavior of wooden members may be required.

Bibliography

[1] Abramowitz, Milton and Irene A. Stegun, 1965, *Handbook of Mathematical Functions*, Dover Publications, Inc., New York.

[2] Bazan, I.M.M., 1980, *Ultimate Bending Strength of Timber Beams*, Ph. D. thesis Dissertation, Nova Scotia Technical College, Halifax, N.S.

[3] Bender, D.A., F.E. Woeste, E.L. Schaffer and C.M. Marx, 1985, *Reliability formulation for the strength and fire endurance of glued-laminated beams*, USDA Forest Service Research Paper FPL 460, U.S. Forest Products Laboratory, Madison, WI.

[4] Bechtel, S.C. and C.B. Norris, 1952, *Strength of Wood Beams and Rectangular Cross-section as affected by Span-Depth Ratio* USDA Forest Service, Forest Product Laboratory Report, M.R1910.

[5] Buchanan, Andrew H., 1984, *Strength Model and Design Methods for Bending and Axial Load Interaction in Timber Members*, thesis presented to the Unversity of British Columbia, at Vancouver, B.C., in partial fulfilment of the requirements for the degree of Doctor of Philosophy.

[6] Chen, W.F. and Atsuta, T., 1976, *Theory of Beam-Columns, Vol. 2, Space behavior and design*, McGraw-Hill Book Company, New York.

[7] Colling, François., 1988, *Estimation of the effect of different grading criterions on the bending strength of glulam beams using the "Karlsruhe calculation model"*, paper presented at IUFRO Wood Engineering Group Meeting, Turku, Finland, June 1988.

[8] Dawe, P.S., 1964, *The Effect of Knot Size on the Tensile Strength of European Redwood*, Wood 29(11):pp 49-51.

[9] Foschi, Ricardo O. and Barrett, David J., 1980, *Glued-Laminated Beam Strength: A Model* Journal of the Structural Division, American Society of Civil Engineers, Vol. 106, No. ST8, August, 1980, pp. 1735–1754.

[10] Foschi, Ricardo O., 1987, *A procedure for the determination of localized modulus of elasticity*, Holz als Roh- und Werkstoff 45 (1987), pp. 257–260.

[11] Foschi, Ricardo O. and Barrett David J., 1976, *Longitudinal shear strength of Douglas-fir*, Canadian Journal of Civil Engineering, Vol. 3, No. 2, June 1976, pp. 198–208.

[12] Foschi, Ricardo O., 1977, *Longitudinal shear strength in wood beams: a design method*, Canadian Journal of Civil Engineering, Vol. 4, 1976, pp. 363–370.

[13] Gjelsvik, Atle, 1981, *The Theory of Thin Walled Bars*, John Wiley & sons, New York.

[14] Glos,P., 1978, *Berichte zur Zuverlassigkeitstheorie der Bauwerke: Zur Bestimmung des Festigkeitsverhaltens von Brettschichtholz bei Druckbeanspruchung aus Werkstoff-und Einwirkungskenngrossen (Reliability Theory for Timber Structures: Determination of Compression Strength Behaviour of Glulam Components from Interaction of Material Properties)*, Heft 34/1978, Laboratorium für den Konstructiven Ingenieurbau, Technische Universität München.

[15] Goodman, J.R. and J. Bodig, 1970, *Orthotropic Elastic Properties of Wood*, Proc. ASCE 96(ST11):pp 2301-2319.

[16] Johnson, J.W. and R.H. Kunesh, 1975, *Tensile Strength of Special Douglas-fir and Hem-fir 2-inch Dimension Lumber*, Wood and Fiber 6(4):pp 305-318.

[17] Koka, Exaud N., 1987, *Laterally Loaded Wood Compression Members: Finite Element and Reliability Analysis*, M.A.Sc. thesis, October 1987, Department of Civil Engineering, The University of British Columbia, Vancouver, B.C., Canada.

[18] Kunesh, R.H. and J.W. Johnson, 1974, *Effect of Size on Tensile Strength of Clear Douglas-fir and Hem-fir Dimension Lumber*, Forest Product Journal 24(8):pp 32-36.

[19] Kunesh, R.H. and J.W. Johnson, 1972, *Effect of Single Knots on Tensile Strength of* 2×8*-inch Douglas-fir Dimension Lumber*, Forest Product Journal 22(1):pp 32-36.

[20] Malhotra, S.K. and S.J.Mazur, 1971, *Buckling Strength of Solid Timber Columns*, Trans. Eng. Inst. of Canada, published in Eng. Journal 13(A-4):I-VII.

[21] Moe, J., 1961, *The Mechanism of Failure of Wood in Bending*, Publication of International Association for Bridge and Structural Engineering, 21:163-178.

[22] Nemeth,L.J., 1965, *Correlation between Tensile Strength and Modulus of Elasticity for Dimension Lumber*, Proc. *2nd* Symposium on Non-Destructive Testing of Wood, Spokane, Washington, USA.

[23] Norris, C.B., 1955, *Strength of Orthotropic Materials Subjected to Combined Stresses*, USDA Forest Sevices, FPL Report No. 1816.

[24] O'Halloran, M.R., 1973, *Curvillinear Stress-Strain Relationship for Wood in Compression*, Ph. D. thesis, Colorado State University.

[25] Timoshenko S. and Woinowsky-Krieger S., 1959, *Theory of Plates and Shells*, McGraw-Hill Book Company, New York.

[26] Timoshenko, S.P.and Gere, J.M., 1961, *Theory of Elastic Stability*, McGraw-Hill Book Company, New York.

[27] Timoshenko, S.P., 1953, *History of Strength of Material*, McGraw-Hill Book Company, New York.

[28] Taylor, S.E. and Bender D.A., 1987, *Modelling Localized Tensile Strength and MOE Properties in Lumber*, paper presented at the 1987 International Winter Meeting of the American Society of Agricultural Engineers, Paper No. 87-4519.

[29] Ylinen, A., 1956, *A Method of Determining the Buckling Stress and Required Cross-sectional Area for centrally loaded Straight Columns in Elastic and Inelastic Range*, IABSA Publications, 16:529-549.

[30] Zienckiewicz, O.C., 1971, *The Finite Element Method in Engineering Science*, McGraw-Hill Book Company, Londan, England.